Engineering 56 (2026) 130–148

Contents lists available at ScienceDirect

Engineering

journal homepage: www.elsevier.com/locate/eng

Research
6G: From Theory to Practice—Article

Cooperative Sensing for 6G ISAC: Concept, Key Technologies, Performance Evaluation, and Field Trial

Guangyi Liu [a], Lincong Han [a,*], Rongyan Xi [a,*], Liang Ma [a], Zixiang Han [a], Yahui Xue [a], Hanting Zhao [a], Jing Jin [a], Qixing Wang [a], Fei Xu [b]

[a] China Mobile Research Institute, Beijing 100053, China
[b] ZGC Institute of Ubiquitous-X Innovation and Applications, Beijing 100080, China

ARTICLE INFO

Article history:
Received 10 December 2024
Revised 18 July 2025
Accepted 27 August 2025
Available online 3 September 2025

Keywords:
Sixth generation
Integrated sensing and communication
Cooperative sensing
Synchronization
Data fusion
Field trial

ABSTRACT

Cooperative integrated sensing and communication (ISAC), an advanced version of ISAC, is becoming an inevitable paradigm in sixth-generation mobile information networks. Based on the foundation of large-scale deployed mobile networks, cooperative ISAC holds promise to realize ubiquitous sensing, thus becoming a significant step in promoting the transformation from connected things to connected intelligence. In this paper, we depict a sweeping panorama of cooperative ISAC, including the concept, key technologies, a performance evaluation framework, and field trials. We start by introducing the application scenarios of cooperative ISAC, which are the motivation for its commercialization. Next, from the perspective of technical development, we trace the evolution of cooperative ISAC, noting that cooperation within sensing and communication is an objective trend. We reveal the four core features of cooperative ISAC—denoted herein as network-enabled, integration, cooperation, and everything—and provide a general system model. Regarding key technologies, we introduce our contributions to antenna array design, cooperative clustering, synchronization, and data fusion, as well as interference management and networking. We also propose an evaluation framework and define several key performance indicators for cooperative ISAC. Through system-level simulations and field trials, we show the practical application feasibility of cooperative ISAC. Finally, we provide guidance on future research directions in cooperative ISAC.

© 2025 THE AUTHORS. Published by Elsevier LTD on behalf of Chinese Academy of Engineering and Higher Education Press Limited Company. This is an open access article under the CC BY-NC-ND license (http://creativecommons.org/licenses/by-nc-nd/4.0/).

1. Introduction

From their first generation (1G) to fifth generation (5G), mobile communication networks have developed rapidly, with communication as a basic network functionality undergoing continuous enhancement. In 5G, three main application scenarios are supported: enhanced mobile broadband (eMBB), massive machine-type communications (mMTC), and ultra-reliable low-latency communication (URLLC) [1]. As we progress toward the sixth generation (6G), numerous new scenarios and services are emerging, including super-powered transportation, holographic communication, enhanced reality, smart manufacturing, and more, which motivate the transformation of mobile communication networks into mobile information networks [2–4]. To support these new requirements and services, sensing is regarded as a new and indispensable functionality for 6G. According to the International Telecommunication Union (ITU), integrated sensing and communication (ISAC) is one of the six main and vital usage scenarios in 6G [5]. As one of the key features in 6G, ISAC has achieved inevitable momentum. The new applications described above require ubiquitous high-accuracy sensing, which will be introduced below. Moreover, sensing and communication technologies are moving along a similar path, resulting in an unstoppable trend toward their integration, which will be introduced in detail in Sections 1.1 and 1.2.

ISAC is expected to furnish various application scenarios (e.g., living, manufacturing, transportation, and social governance) with sensing capabilities such as detection, localization, identification, and imaging [6]. As shown in Fig. 1, ISAC can provide services for smart living, including intelligent home control, security monitoring, and accident detection [7]. Medical healthcare also requires high-accuracy and real-time sensing for applications such as breath and heartbeat monitoring and spectrum examinations [8].

* Corresponding authors.
E-mail addresses: hanlincong@chinamobile.com (L. Han), xirongyan@chinamobile.com (R. Xi).

https://doi.org/10.1016/j.eng.2025.08.033
2095-8099/© 2025 THE AUTHORS. Published by Elsevier LTD on behalf of Chinese Academy of Engineering and Higher Education Press Limited Company.
This is an open access article under the CC BY-NC-ND license (http://creativecommons.org/licenses/by-nc-nd/4.0/).

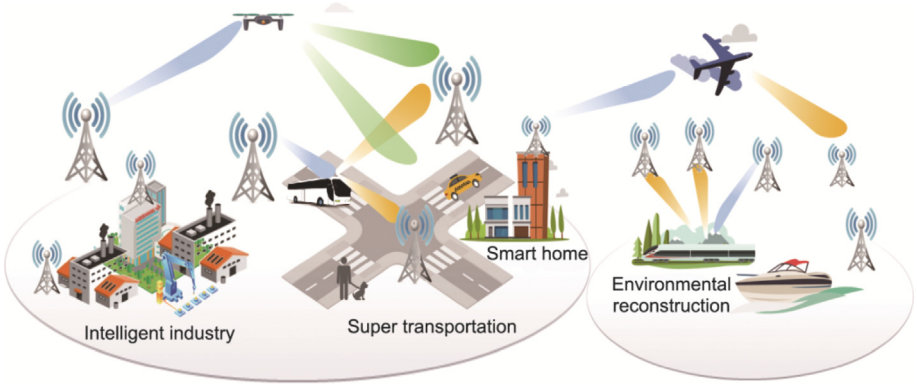

Fig. 1. ISAC application scenarios.

For the industrial Internet of Things (IIoT), ISAC can assist in the automation of mechanical equipment and robotic devices [9]. For transportation, ISAC can be used to detect unauthorized unmanned aerial vehicles (UAVs) or supervise UAV flight trajectories, thereby supporting a scale expansion of the low-altitude economy [10]. For ground transportation (e.g., vehicle-to-everything (V2X)), ISAC can outperform automotive radar, in that it can avoid blind areas caused by occlusion between vehicles [11]. Traffic flow can also be sensed and monitored by networks, and traffic command can be dynamically adjusted in real time [12]. For social governance, ISAC can provide environmental monitoring benefits, in that various sensors and network devices can monitor rainfall, the atmosphere, air pollution, and so forth. Through environmental reconstruction, ISAC can also increase public security in applications such as security examinations and electronic fences [13,14].

1.1. Historical view of cooperative ISAC

Research interest in ISAC has increased in recent years, based on a dual motivation of scenarios and technologies, as mentioned above. Two research directions have gradually emerged in this field: cooperative ISAC and non-cooperative ISAC. In non-cooperative ISAC, only one transceiver is used to both transmit sensing signals and receive the echo signals reflected from the target, based on the sensing topology of monostatic sensing. The signal band is also single. In contrast, cooperative ISAC utilizes multiple sensing transmitters (Txs) and receivers (Rxs), multiple bands, and even multiple types of devices. Cooperative ISAC has been demonstrated to offer accuracy gain and reliability gain; thus, it is regarded as a solution to a systematic optimization that realizes a trade-off among functional capability, resource efficiency, and network quality. To specifically illustrate the necessity of cooperative ISAC in 6G and beyond, we outline the evolution of cooperative ISAC in this subsection; the timeline is provided in Fig. 2.

1.1.1. From monostatic radar to distributed MIMO radar

First proposed in the 1930s, at the beginning of radar research, monostatic radar is the foundational sensing mode in radar systems [15]. This mode is straightforward and easy to operate, as synchronization can be omitted. However, monostatic radar has limitations in terms of sensing coverage, multi-target identification, and more. To address these defects, the idea of bistatic radar was proposed in 1952 by Keeve Milton Siegel and Robert Engel Machol, and was sequentially developed into multistatic radar [16,17]. These two modes contain multiple separately located Txs and Rxs. The rise of bistatic/multistatic radar spawned many related technologies, such as data fusion, triangular measurements, and multi-observation imaging [18–20]. Multiple-input multiple-output (MIMO) is a communication technique first created in 1994 [21]. Attracted by its spatial diversity gain, researchers from the Massachusetts Institute of Technology (MIT) Lincoln Laboratory introduced MIMO into radar systems in 2003 [22]. Under different sensing modes, Txs and Rxs were henceforth able to be equipped with multiple co-located antenna arrays. Five years later, distributed MIMO radar was introduced by researchers from Zhejiang University [23]. Distributing the locations of both the Txs/Rxs and the antennas and coordinating them gave radar systems high resolution and strong anti-jamming capability [24]. From monostatic radar to distributed MIMO radar, a trend of cooperative sensing can be observed throughout the research progression of radar theory.

1.1.2. From MIMO to cell-free MIMO

As mentioned above, MIMO is a key technology in communication networks. Over the past three decades, MIMO has been improved to realize the features of distribution and cooperation. In 2008, coordinated multiple point (CoMP) was proposed for the first time by Ericsson in the 53rd meeting of the 3rd Generation Partnership Project (3GPP) Radio Access Networks Working Group 1 (RAN1) [25]. In CoMP, multiple nodes are connected by fibers to provide communication service for a single piece of user equipment (UE), particularly cell edge UEs [26]. Distributed MIMO and cell-free MIMO can be regarded as extensions of traditional MIMO, in that they break cell boundaries and provide user-centric communication services [27–29]. Moreover, the distribution of communication nodes can be made denser and more dynamic [30].

1.1.3. From dual-functional radar and communication to cooperative ISAC

Due to the natural similarities between communication and sensing (e.g., signal processing), the study of their interplay has progressed for 60 years. Early on, researchers and engineers in the field of radar tried to embed communication signals into radar systems, mainly to assist in military surveillance [31–38]. These kinds of systems are called dual-functional radar and communication (DFRC) or joint radar and communication (JRC). In Ref. [31], a method of modulating the data bits on intervals between radar pulses is designed. Researchers have used chirp-based radar waveform to carry communication information by using the data bits to modulate the chirp signals' degrees of freedom (e.g., amplitude, frequency, and phase) [32,33]. Communication bits can also be conveyed by acting as the controller of the radar waveform's sidelobe [34].

Aside from traditional types of radar waveform, orthogonal frequency-division multiplexing (OFDM), which was proposed for

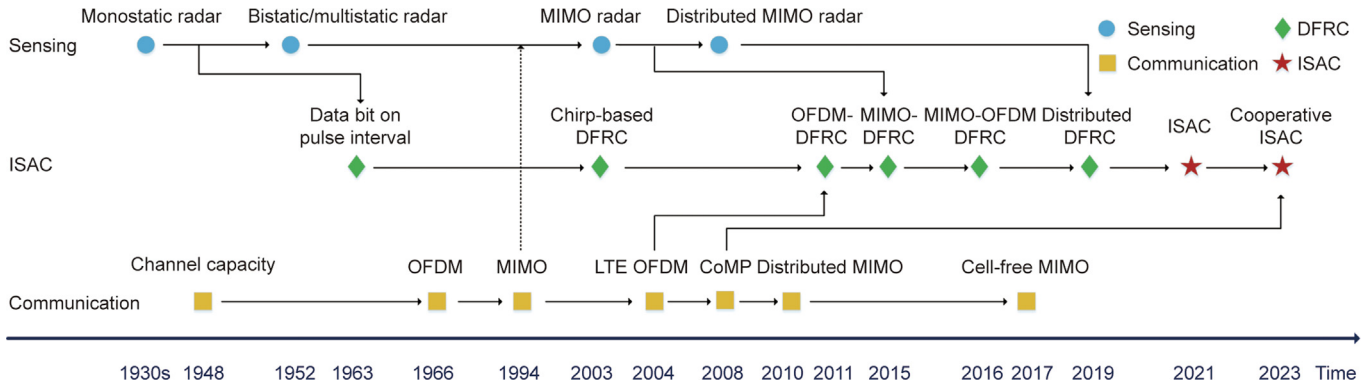

Fig. 2. Developing trends in cooperative ISAC. MIMO: multiple-input multiple-output; OFDM: orthogonal frequency-division multiplexing; DFRC: dual-functional radar and communication; LTE: long-term evolution; CoMP: coordinated multiple points.

communication and then standardized in long-term evolution (LTE) in 2004, gradually became a popular waveform for radar and DFRC [35,36]. OFDM-DFRC then developed into MIMO-OFDM DFRC and distributed DFRC in 2016 and 2019, respectively [37,38]. With increasing demand for sensing in commercial applications, and given the similar development trends of communication and sensing, ISAC has generally attracted research interest in the field of communication. Scholars have found that 5G networks and beyond with large-scale nodes are suitable for embedding sensing functionality; in 2021, such a system was first denoted as "ISAC" [39,40]. The past three years have seen unprecedented enthusiasm for the study of ISAC, which has been researched and applied in 5G-advanced (5G-A) networks. However, the 5G-A version of ISAC is monostatic, being single-modal and single-band. Monostatic ISAC is limited by severe self-interference and low line-of-sight (LoS) probability [41]. Single modal means that only the base stations (BSs)' radio signals are used for sensing, which does not work well for object imaging and recognition scenarios [14]. In addition, ISAC in 5G-A mainly focuses on a single band, such as sub-6 GHz, which ensures sensing coverage but does not have a fine enough beamwidth to provide high angular resolution. To solve these problems, considering that sensing and communication architectures are tending toward cooperation, and in order to be more compatible with existing cellular networks, operators such as China Mobile proposed the concept of cooperative ISAC in 2023 [42,43], aiming to make full use of large-scale deployed networks to realize ubiquitous sensing with much less complex implementation at the BS.

1.2. Cooperative ISAC: A novel and inevitable paradigm for 6G

Based on the discussion of the trend of ISAC in the previous subsection, we draw the conclusion that cooperative ISAC has become a novel and inevitable paradigm, compared with the traditional communication-only, radar-only, and basic ISAC paradigms, and will play an increasingly significant role in 6G and beyond. We have witnessed the birth of cooperative ISAC, which is still in its early stage and not yet mature enough for commercialization. Many technical challenges remain to be faced, attracting numerous researchers' interests and efforts. In this subsection, we identify these challenges and discuss the corresponding representative research progress in the past two years.

- **Channel modeling.** Current channel modeling methods and specifications—such as 3GPP TR 38.901, which focuses on communication channels—will not be adaptive to the characteristics of a 100% cooperative sensing channel [44,45]. For example, if the channel from the Tx to the Rx is divided into two segments by the targets, the modeling of the targets' radar cross-section (RCS) will be missed [46]. Therefore, researchers have proposed novel channel modeling schemes such as the shared cluster-based stochastic channel model [47] and the deterministic ray-tracing model [48]. In Ref. [43], the RCS of bistatic sensing and that of monostatic sensing are compared, revealing that bistatic sensing is more likely to obtain a higher RCS of the target than monostatic sensing.
- **Coverage enhancement.** To reuse current cellular networks for sensing, coverage is an essential issue that must be addressed. In comparison with communication UEs, sensing targets are more widely distributed in the space. Although cooperative sensing can achieve wider coverage than non-cooperative sensing (e.g., monostatic sensing), problems remain. For example, how can the sensing area for each sensing cluster be divided to achieve seamless sensing coverage, and how can appropriate antenna arrays and beam patterns be designed for different sensing requirements? Li et al. [49] proposed a beamforming optimization algorithm to improve the signal-to-interference-plus-noise ratio (SINR) of targets in the edge sensing areas. Considering both communication and sensing, a unified metric named "coverage probability" is designed in Ref. [50], and its limitations under overall resource constraints are analyzed.
- **Clustering and data fusion.** The topology of cooperative sensing directly influences the sensing accuracy gain and geometry gain [51]. Lu et al. [52] proposed a deep-learning-based multi-node ISAC system to realize four-dimensional (4D) environmental construction by means of uplink–downlink cooperation. Macro–micro cooperation is also considered in node-deployment in Ref. [53]. In Ref. [54], both multi-BS cooperation and BS–UE cooperation are considered. Stochastic geometry is another popular tool to help determine node distribution, as studied in Ref. [55].
- **Imperfection mitigation.** Non-ideal issues concerning synchronization, non-line-of-sight (NLoS) propagation, and clutter contamination are regarded as having a negative effect on sensing accuracy. A round-trip method has been proposed to avoid the influence of timing error when estimating delay [56], and the clutter-suppression issue is addressed in Ref. [57]. For NLoS cases, Wang et al. [41] proposed a joint angle-of-arrival (AoA) and angle-of-departure (AoD) estimation algorithm that can simultaneously estimate the location of the target and the scatterer. Deeper research is still required on frequency, phase synchronization, and multi-scatterer multi-target NLoS mitigation.
- **Interference management and networking.** Cooperative ISAC brings the advantages of wide-spread and large-scale nodes, although these may cause interference between different nodes, clusters, or functions. Therefore, interference elimination is a key issue that directly influences network quality [58]. Many

researchers have made contributions on this topic. Liu et al. [43] revealed that intra-site interference is much greater than inter-site interference, so networking schemes among multiple cells must be properly designed. In Ref. [59], interference mitigation is realized by appropriate node selection. Beamforming design and power control are also vital schemes to eliminate the power of interference signals [60–63].

A summary of the challenges and the corresponding research progress is shown in Table 1 [41,43,47–63].

1.3. Structure of this paper

In this paper, we provide a comprehensive technical overview of the concept, key technologies, performance evaluation, and field trials of cooperative ISAC, as shown in Fig. 3. The concept, which is summarized as "NICE" (where "N" stands for network-enabled, "I" stands for integration, "C" stands for cooperation, and "E" stands for everything), and a system model of cooperative ISAC are proposed in Section 2. Section 3 introduces key technologies in cooperative ISAC, including antenna array design, cooperative clustering, synchronization, and data fusion. An evaluation framework for key performance indicators (KPIs) of cooperative ISAC is established in Section 4. Section 5 provides system-level performance evaluation results of cooperative sensing in ISAC. Field trial procedures and results are shown in Section 6. Section 7 points out several future directions for cooperative ISAC, and Section 8 concludes the paper. The main differences between prior works and this article are listed in Table 2 [6,9,39,40,43,49,50,64,65].

2. Concept and system model

2.1. Concept of cooperative ISAC

Conventionally, based on radar theory and according to topology, there are four types of sensing modes: monostatic, multiple monostatic, bistatic, and multistatic. As the first mode involves only one sensing transceiver, it can be classified as non-cooperative sensing. The other three require cooperation between different Txs or Rxs, so they can be classified as cooperative sensing. However, by embedding the sensing function into mobile communication networks, and with the development of ISAC, the concept and scope of cooperative ISAC is greatly extended. In this paper, we summarize the core features of cooperative ISAC using the acronym "NICE." The specific meaning of each feature is explained below.

(1) **Network-enabled.** In recent decades, the scale of mobile communication networks has expanded at an extraordinary speed, resulting in ubiquity as a key feature. Unlike traditional radar systems, which were only deployed in certain limited, permitted areas, densely spread BSs can act as both communication and sensing access points (APs), exponentially expanding sensing coverage. By relying on the current centralized radio access network (C-RAN) and on future new network architectures such as cell-free architecture, it will be possible to quickly transmit and collect sensing information, ensuring the requirements of low-latency sensing services such as intrusion detection and collision detection in UAV and V2X scenarios. 6G networks are undergoing a transformation from mobile communication networks to mobile information networks, in which computing becomes an important support power. Sensing will also benefit by using networks' computing function to provide more intelligent sensing results and instructions in many scenarios, including intelligent indoor factories and homes.

(2) **Integration.** Integration reflects two aspects: network functions and information fusion. In terms of network functions, communication and sensing will be integrated into the same mobile networks, sharing the same network infrastructures, software, or hardware. For software, the wireless resources in at least one domain (time, frequency, spatial, code, or power) will be shared by the two functions. For hardware, the two functions of communication and sensing will be able to share the same antenna arrays. In terms of information fusion, sensing information will be fused at three levels—namely, the signal level, symbol level, and data level—respectively integrating the information in raw signals, mid-process sensing results (e.g., delay, angle, and Doppler spread), and final sensing results (e.g., range, position, and velocity). The complexity of these three levels will decrease, but the estimation error will increase.

(3) **Cooperation.** There are three dimensions of cooperation: multi-node, multi-band, and multi-function cooperation. First of all, multi-node cooperation, in which multiple Txs and Rxs jointly accomplish sensing or communication missions, coherently or non-coherently, is vital, as it can improve both the sensing accuracy of edge targets and the data rate of edge UEs. Moreover, compared with single-node sensing, which requires expensive hardware upgrading to remove self-interference effects when receiving echo signals, bistatic and multistatic sensing can largely

Table 1
Current key research directions in cooperative ISAC.

Category	Specific methods	References	Representative progress
Channel modeling	Stochastic channel model	[47]	Shared clusters observed between the target channel and background channel
	Deterministic ray-tracing model	[48]	A ray-tracing channel model proposed for terahertz-ISAC
	RCS modeling	[43]	Bistatic sensing proved to have a greater probability of obtaining a higher RCS
Coverage enhancement	Beamforming to ensure edge target sensing	[49]	Seamless sensing coverage achieved in the prescribed region
	Coverage probability analysis	[50]	Denser networks proved to significantly enhance ISAC coverage
Clustering and data fusion	Cooperation gain analysis	[51]	Cooperative sensing proved to offer accuracy gain and geometry gain
	Uplink–downlink cooperation	[52]	A clustering method proposed for 4D environment construction
	Macro–micro cooperation	[53]	A node-deployment scheme suggested based on macro or micro nodes
	BS–UE cooperation	[54]	BS and UE selected as sensing pairs
	Stochastic geometry	[55]	Node location optimized using stochastic geometry
Non-ideal condition mitigation	Synchronization	[56]	Round-trip measurement proposed to avoid timing error
	Clutter suppression	[57]	A clutter-elimination method proposed
	NLoS mitigation and exploitation	[41]	Both the target and the scatterer that cause NLoS located
Interference management and networking	Networking coordination	[58,59]	Interference avoided through appropriate node choice
	Beam and waveform design	[60,61]	Schemes such as nulling proposed to stop signals from being transmitted in directions that will cause interference
	Power control	[62,63]	Power of the interference signal controlled to eliminate interference

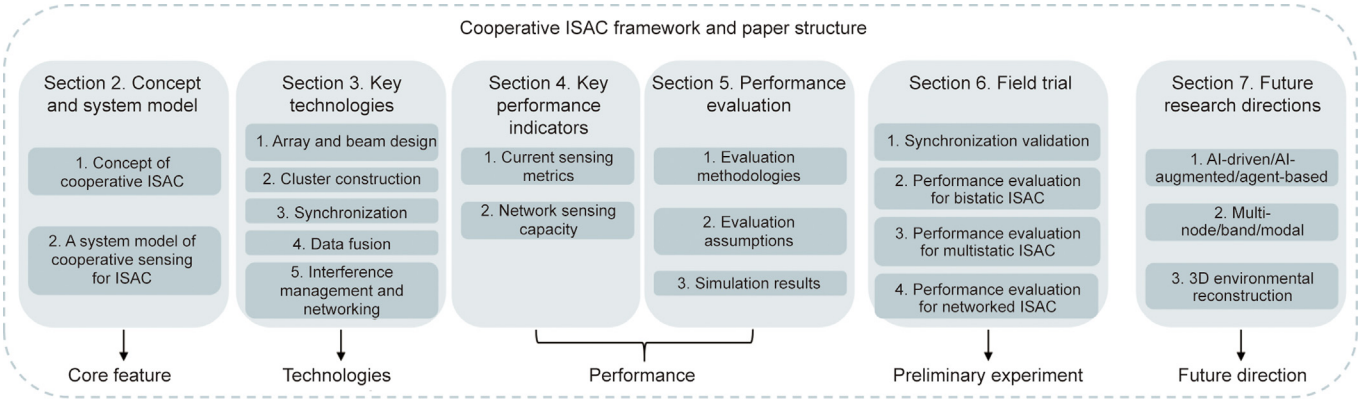

Fig. 3. Cooperative ISAC framework and the structure of this paper.

Table 2
Overview of existing work on cooperative ISAC, compared with the present paper.

Reference	Year	Key technologies	KPI	Performance evaluation	Field trial	Cooperative ISAC
[6]	2024	①③④⑤	×	√	×	×
[9]	2024	①③	×	×	×	×
[39]	2021	①②	×	×	×	×
[40]	2022	①③⑤	√	×	×	×
[43]	2024	③⑤	×	√	√	√
[49]	2024	②③④	×	√	×	×
[50]	2024	④	×	√	×	×
[64]	2024	②⑤	√	√	×	×
[65]	2025	②③④	×	√	×	√
This paper	2025	①②③④⑤	√	√	√	√

① Array and beam design; ② cluster construction; ③ data fusion; ④ synchronization; ⑤ interference management and networking.

avoid self-interference naturally. Secondly, multi-band cooperation is also important, as 6G will be a full-spectrum system with a combination of low-, middle-, and high-frequency bands. The low-frequency band will enable wide coverage, to meet the basic communication rate of megabits per second. In addition, wide-area passive Internet of Things (IoT) technology can be utilized to realize the sensing of tagged devices. The mid-frequency band (sub-10-GHz band) will mainly be used for continuous coverage, data rates in gigabits per second, and sensing accuracy in the coarse-granularity (meter-level) range. The high-frequency band (i.e., millimeter-wave, terahertz, and visible light) will be able to be turned on on-demand, further improving the communication rate and sensing resolution. Finally, communication and sensing can assist each other to obtain synergistic effects. Sensing can enhance communication quality in procedures such as pilot contamination elimination and beam alignment; its modeling of the surrounding environment can also provide channel information for communication. In turn, sensing can benefit from communication in using data signals or reference signals to locate targets, as well as in transmitting sensing information by means of BSs or UEs. These two functions therefore form a positive feedback loop.

(4) **Everything.** In 6G cooperative ISAC systems, there will be numerous devices and equipment that can serve as sensing Txs and Rxs, including BSs, UEs, and various kinds of sensors. With the evolution of mobile network standardization, such as sidelinks and Xn interfaces, BS–BS, BS–UE, and UE–UE sensing pairs will all be supported. The advantages of BSs include large antenna panels and adequate power, while those of UEs include high mobility and dense distribution. Abundant sensors will also be able to provide multiple types of sensing information, including image, temperature, precipitation, infrastructure micro-deformation, and so forth, making multi-source multi-modal sensing possible.

2.2. A system model of cooperative sensing for ISAC

In cooperative sensing systems, Txs and Rxs can be BSs, UEs, or other kinds of devices and sensors, under different sensing scenarios and service requirements. Fig. 4 shows an example of the system topology of a cooperative sensing system based on cellular networks. First, for UAVs flying at low altitudes, the sensing Txs and Rxs are mainly BSs, since the distances from the Txs/Rxs to the UAVs are extremely large (~500 m), requiring high transmission power to transmit strong enough sensing signals and large antenna arrays to ensure the necessary angular resolution. For ground vehicles, in addition to BSs, Tx micro-BSs (TmBSs) and UEs can serve as sensing Txs/Rxs, contributing to the real-time tracking and orientation estimation of quickly moving vehicles. As shown in Fig. 4, both Tx BSs (TBSs) and TmBSs transmit sensing

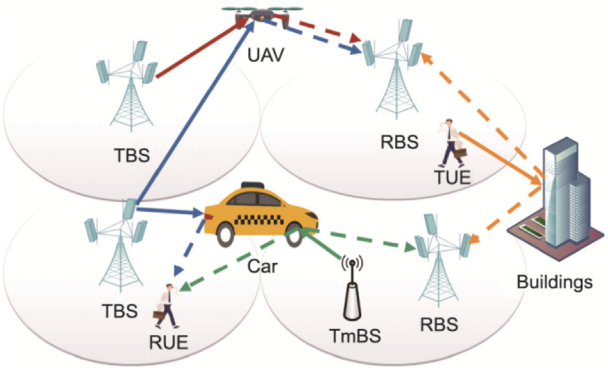

Fig. 4. System model of cooperative sensing in an ISAC system. TBS: Tx BS; RBS: Rx BS; TUE: Tx UE; RUE: Rx UE; TmBS: Tx micro-BS.

signals to vehicles, while echo signals are received by both Rx UEs (RUEs) and Rx BSs (RBSs). Thirdly, it is necessary to sense environmental objects, in that environmental information can assist in road-condition monitoring, factory robot instruction, data signal propagation, and so forth. Fig. 4 shows a case of Tx UEs (TUEs) and RBSs serving as Txs and Rxs, respectively.

In this section, we consider a cooperative sensing system with multiple sensing Txs and Rxs using MIMO and OFDM technologies. When establishing the system model, we are only interested in the parameter settings of the Txs and Rxs, rather than differentiating between their type. We assume that there are M Txs transmitting sensing signals to G targets, whose reflected echo signals are received by N Rxs. The locations of the mth Tx and the nth Rx are denoted by $\boldsymbol{p}_{\mathrm{T},m}=[x_{\mathrm{T},m},\ y_{\mathrm{T},m}]^{\mathrm{T}}$ and $\boldsymbol{p}_{\mathrm{R},n}=[x_{\mathrm{R},n},\ y_{\mathrm{R},n}]^{\mathrm{T}}$, respectively, where $x_{\mathrm{T},m}$ and $y_{\mathrm{T},m}$ represent the x-coordinate and y-coordinate of the mth Tx with $m=1,\ldots,M$, respectively, $x_{\mathrm{R},n}$ and $y_{\mathrm{R},n}$ represent the x-coordinate and y-coordinate of the nth Rx with $n=1,\ldots,N$, respectively. The unknown location of the gth target is $\boldsymbol{p}_g=[x_g,\ y_g]^{\mathrm{T}}$, where x_g and y_g represent the x-coordinate and y-coordinate of the gth target with $g=1,\ldots,G$. All the Txs and Rxs are equipped with a uniform linear array (ULA). The antenna number of each Tx and Rx is denoted by $L_{\mathrm{T},m}$ and $L_{\mathrm{R},n}$, respectively, and the distance between two adjacent antennas is denoted by d.

2.2.1. Transmission model

The central carrier frequency is f_{c} and the wavelength is $\lambda_{\mathrm{c}}=c/f_{\mathrm{c}}$, where c is the speed of light. For the mth Tx, the bandwidth is BW_m. Suppose that the transmitted signal in one OFDM resource grid, denoted by $\boldsymbol{s}_{\mathrm{T},m}$, contains I_m subcarriers and K_m symbols in —that is, $I_m\times K_m$ resource elements (REs) in total. The transmitted signal at the $[i_m,\ k_m]$th RE, denoted by $\boldsymbol{s}_{\mathrm{T},m}[i_m,\ k_m]^{\mathrm{T}}$, forms the normalized complex Gaussian distribution with a zero-mean and covariance $\mathbb{E}\left[\|\boldsymbol{s}_{\mathrm{T},m}[i_m,\ k_m]\|^2\right]=1$, where $\mathbb{E}[\cdot]$ denotes the expectation operator, which has the following form:

$$\boldsymbol{s}_{\mathrm{T},m}[i_m,\ k_m]^{\mathrm{T}}=\left[\boldsymbol{s}_{\mathrm{T},m}^{(1)}[i_m,\ k_m],\ldots,\boldsymbol{s}_{\mathrm{T},m}^{(Q_m)}[i_m,\ k_m]\right]^{\mathrm{T}} \tag{1}$$

where $i_m=0,\ldots,I_m$, $k_m=1,\ldots,K_m$, and Q_m is the number of transmitted beams at the mth Tx.

Beamforming methods can be fully digital, fully analog, or hybrid. Here we select hybrid beamforming as an example. The beamforming matrix can be expressed as $\boldsymbol{F}_m[i_m,\ k_m]=\boldsymbol{F}_m^{\mathrm{RF}}\boldsymbol{F}_m^{\mathrm{BB}}[i_m,\ k_m]\in\mathbb{C}^{L_{\mathrm{T},m}\times Q_m}$, which consists of the high-dimension analog beamforming matrix $\boldsymbol{F}_m^{\mathrm{RF}}\in\mathbb{C}^{L_{\mathrm{T},m}\times L_{\mathrm{RF}}}$ and the low-dimensional digital beamforming matrix $\boldsymbol{F}_m^{\mathrm{BB}}[i_m,\ k_m]\in\mathbb{C}^{L_{\mathrm{RF}}\times Q_m}$, respectively, where L_{RF} is the number of the radio frequency (RF) chains and $\mathbb{C}$ represents the complex number set. Under normalized directional beamforming, $\boldsymbol{F}_m[i_m,\ k_m]$ can be expressed as $\boldsymbol{F}_m[i_m,\ k_m]=1/\sqrt{Q_m}[\boldsymbol{f}_{m,1},\ldots,\boldsymbol{f}_{m,Q_m}]^{\mathrm{T}}$, where the q_mth $(q_m=1,\ldots,Q_m)$ beam $\boldsymbol{f}_{m,q_m}$ is expressed as

$$\boldsymbol{f}_{m,q_m}=\frac{1}{\sqrt{L_{\mathrm{T},m}}}\left[1,\ldots,\mathrm{e}^{\mathrm{j}(L_{\mathrm{T},m}-1)2\pi d\psi_{q_m}/\lambda_{\mathrm{c}}}\right]^{\mathrm{T}} \tag{2}$$

with ψ_{q_m} standing for the corresponding phase of $\boldsymbol{f}_{m,q_m}$ and j is the square root of −1.

2.2.2. Channel model

The channel matrix from the mth Tx to the gth target, and then from the target to the nth Rx, in the i_mth subcarrier, k_mth symbol, is written as $\boldsymbol{H}_{m,n,g}[i_m,\ k_m]$ and can be expressed as

$$\boldsymbol{H}_{m,n,g}[i_m,\ k_m]=h_{m,n,g}\sqrt{\beta_{m,n,g}}\,\mathrm{e}^{-\frac{\mathrm{j}2\pi i_m\tau_{m,n,g}}{I_mT_{\mathrm{s}}}}\mathrm{e}^{\mathrm{j}2\pi f_{\mathrm{D},m,n,g}k_mT_{\mathrm{s}}}\boldsymbol{a}_{\mathrm{R}}\left(\varphi_{n,g}\right)\boldsymbol{a}_{\mathrm{T}}^{\mathrm{H}}(\theta_{m,g}) \tag{3}$$

where $\beta_{m,n,g}$ is the path loss, T_{s} is the sampling duration, $\tau_{m,n,g}$ is the propagation duration of the whole path, $f_{\mathrm{D},m,n,g}$ is the Doppler spread caused by the velocity, and $h_{m,n,g}=h_{m,n,g}^{\mathrm{R}}+\mathrm{j}h_{m,n,g}^{\mathrm{I}}$ is the complex channel gain, containing the real part $h_{m,n,g}^{\mathrm{R}}$ and the imaginary part $h_{m,n,g}^{\mathrm{I}}$. The antenna steering vector $\boldsymbol{a}_{\mathrm{R}}\left(\varphi_{n,g}\right)\in\mathbb{C}^{L_{\mathrm{R},n}\times 1}$ and response vector $\boldsymbol{a}_{\mathrm{T}}(\theta_{m,g})\in\mathbb{C}^{L_{\mathrm{T},m}\times 1}$ containing the AoA $\varphi_{n,g}$ at the nth Rx and the AoD $\theta_{m,g}$ at the mth Tx respectively can be expressed as

$$\boldsymbol{a}_{\mathrm{T}}(\theta_{m,g})=\frac{1}{\sqrt{L_{\mathrm{T},m}}}\left[1,\ldots,\mathrm{e}^{\mathrm{j}(L_{\mathrm{T},m}-1)2\pi d\sin\theta_{m,g}/\lambda_{\mathrm{c}}}\right]^{\mathrm{T}} \tag{4}$$

$$\boldsymbol{a}_{\mathrm{R}}\left(\varphi_{n,g}\right)=\frac{1}{\sqrt{L_{\mathrm{R},n}}}\left[1,\ldots,\mathrm{e}^{\mathrm{j}(L_{\mathrm{R},n}-1)2\pi d\sin\varphi_{n,g}/\lambda_{\mathrm{c}}}\right]^{\mathrm{T}} \tag{5}$$

The path loss $\beta_{m,n,g}$ is decided by the wavelength, the RCS of the gth target σ_g, the distance from the mth Tx to the target $d_{m,g}$, and the distance from the target to the nth Rx $d_{g,n}$:

$$\beta_{m,n,g}=\frac{\sigma_g\lambda_{\mathrm{c}}^2}{(4\pi)^3d_{m,g}^2d_{g,n}^2} \tag{6}$$

2.2.3. Received model

After OFDM demodulation, the echo signal reflected by the gth target, received at the nth Rx from the mth Tx for the $[i_m,\ k_m]$ th RE, is denoted as $\boldsymbol{y}_{m,n,g}[i_m,\ k_m]$ and given by the following:

$$\begin{aligned}\boldsymbol{y}_{m,n,g}[i_m,\ k_m]=&\sqrt{P_m}\boldsymbol{H}_{m,n,g}[i_m,\ k_m]\boldsymbol{F}_m[i_m,\ k_m]\boldsymbol{s}_{\mathrm{T},m}[i_m,\ k_m]\\&+\boldsymbol{w}_{m,n,g}[i_m,\ k_m]\end{aligned} \tag{7}$$

where P_m is the transmission power of the mth Tx and $\boldsymbol{w}_{m,n,g}[i_m,\ k_m]$ is the noise vector forming the circularly symmetric complex normal distribution.

3. Key technologies

3.1. Array and beam design

As the critical interface between wireless systems and the environment, antenna arrays play a pivotal role in the performance of ISAC systems. To meet the requirements of wide-area coverage and high-resolution sensing, wide-angle antennas are essential. However, a large-scale antenna and its RF can be expensive. Thus, the key issue of how to design appropriate antenna arrays and codebooks for different sensing areas requires investigation.

3.1.1. Array-scale selection

Sensing accuracy has a strong relationship with the antenna array. The larger the antenna array aperture, the finer the beamwidth. The beamwidth then influences the angular resolution and angle estimation accuracy. If a 3 dB beamwidth under a certain antenna array is denoted by $W_{3\mathrm{dB}}$, then the angular resolution θ_{r} and angle estimation accuracy ε_θ can be obtained as follows:

$$\theta_{\mathrm{r}}\approx 0.886\frac{\lambda_{\mathrm{c}}}{W_{3\mathrm{dB}}},\ \varepsilon_\theta\approx\frac{\theta_{\mathrm{r}}}{1.6\sqrt{\mathrm{SINR}}} \tag{8}$$

We provide an example of the current normal antenna array settings in 5G in Table 3 to demonstrate the limitations on realizing high-accuracy location estimation. It can be calculated that the beamwidth is around 6°; then, the corresponding angle estimation accuracy ε_θ and localization error ε_{r} are around 0.5° and 23.19 m (at a range of 1200 m), respectively, which are too large to satisfy the sensing accuracy demand of below 20 m or even 10 m.

To ensure sensing accuracy, larger-scale antenna arrays will be needed in 6G. However, increasing the scale of antenna arrays will increase the cost. Therefore, the sensing areas should be further defined, and different scales of antenna arrays should be used. For example, consider a low-altitude UAV scenario: When the height range of the UAV is greater, a larger antenna scale with a larger field angle θ_{field} is needed. Therefore, adaptive antenna array scales (corresponding to different values of the antenna number L) can be applied to different sensing areas, as shown in Fig. 5.

3.1.2. Angular coverage

Achieving wide angular coverage is crucial for ISAC systems, as it allows for simultaneous detection and communication with multiple targets. In addition, for UAV-detection scenarios, sensing nodes must cover a large angle along the elevation angle. However, current BSs radiate toward the ground with a positive downtilt angle to provide the best communication coverage. Therefore, the design of an antenna with wide angular coverage is important to ensure both communication and sensing performance. In terms of sensing capabilities, antennas with large angular coverage enable more accurate target detection and tracking by providing a broader field of view and better resolution. This is particularly important in applications such as UAVs, where precise sensing information is critical for safe and effective operation [66]. Additionally, such antennas can support multiple sensing services simultaneously, including radar, light detection and ranging (LiDAR), and imaging, further increasing their versatility and utility. All these requirements call for antennas designed with wide beamwidths and low sidelobe levels to minimize mutual interference among different beams.

Sensing is required to cover multiple kinds of targets, such as UAVs, vehicles, and vulnerable road users (VRUs). It is obvious that these sensing targets will be non-uniformly distributed in the dimension of elevation angles, for example. The whole range of sensing areas can be divided into two kinds: core area and non-core area (Fig. 6). Correspondingly, transmitted and received beams are required to ensure the dual effect of fine-granularity sensing in core areas and coarse-granularity coverage in non-core areas. The current standardization of precoding codebooks, such as the type-I single-panel or multi-panel codebooks in 3GPP, mainly supports uniform beam distribution, which is controlled by the oversampling factor of the first-dimension or second-dimension discrete-Fourier-transform (DFT) vector—that is, O_1 or O_2 [67]. Taking the first dimension as an example, the traditional DFT matrix $\boldsymbol{X}_1 \in \mathbb{C}^{N_1 \times O_1 N_1}$ can be expressed as

$$\boldsymbol{X}_1 = \begin{bmatrix} 1 & 1 & \cdots & 1 \\ 1 & e^{\frac{j2\pi}{O_1 N_1}} & \cdots & e^{\frac{j2\pi(O_1 N_1 - 1)}{O_1 N_1}} \\ \vdots & \vdots & \vdots & \vdots \\ 1 & e^{\frac{j2\pi(N_1 - 1)}{O_1 N_1}} & \cdots & e^{\frac{j2\pi(O_1 N_1 - 1)(N_1 - 1)}{O_1 N_1}} \end{bmatrix} \tag{9}$$

where N_1 is the number of antennas for the first dimension. The DFT matrix can be regarded as uniformly dividing the angle of beams with the range $[0, 2\pi)$ into $O_1 N_1$ values. The relationship between the i_{DFT}th DFT vector in Eq. (9) and the i_{angle}th angle ($\theta_{i_{\text{angle}}}$) when $i_{\text{DFT}} = i_{\text{angle}}$ is

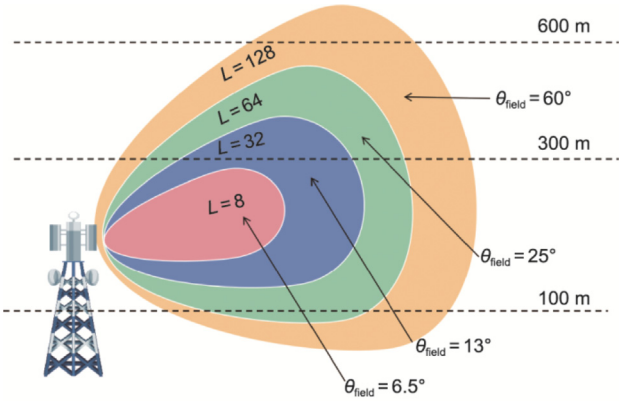

Fig. 5. Different array scales for different sensing areas.

$$\theta_{i_{\text{angle}}} = (i_{\text{angle}} - 1)\Delta\theta = \frac{2\pi(i_{\text{DFT}} - 1)}{N_1 O_1} \tag{10}$$

where $\Delta\theta$ is the angular duration of the adjacent beams.

To generate the non-uniform distributed beam angle, the traditional DFT codebook can be modified by introducing more than one value for the oversampling factors. Specifically, we assume that, according to a certain sensing demand, the whole angular range $[0, 2\pi)$ should be divided into U sets, where each set of angles can have a different angular duration. For the uth angular set (u = 1,..., U), the total number of angles is L_u, the angular duration is $\Delta\theta_u$, and the initial angle is $\theta_{u,0}$. Then, the corresponding oversampling factor is $O_{1,u}$, and the lth angle (l = 1,..., L_u) within the uth angular set is $\theta_{u,l} = \theta_{u,0} + (l-1)\Delta\theta_u$. The initial angle of each angular set has the following relationship:

$$\theta_{u,0} = \begin{cases} 0, & u = 1 \\ \theta_{u-1,L_{u-1}} + \Delta\theta_u, & 1 < u \le U \end{cases} \tag{11}$$

Such a DFT codebook can be generated according to the following procedures:

Step 1: Generate U traditional DFT matrices $\{\boldsymbol{X}_{1,1}, \ldots, \boldsymbol{X}_{1,U}\}$ using U oversampling factors $\{O_{1,1}, \ldots, O_{1,U}\}$.

Step 2: Select L_u columns from the uth traditional DFT matrix to form a modified DFT matrix $\boldsymbol{X}_{\text{Modified},u}$ that is in accordance with the L_u angles in the uth required angular set. Here, a problem arises: The corresponding angular set of the uth traditional DFT matrix may not contain the required angles. For example, we want to obtain the angular set of $\{\pi/12, \pi/4, 5\pi/12\}$ whose angular duration is $\pi/6$ with a corresponding oversampling factor of 6 when the antenna number is 2. However, the traditional angular set that corresponds to the traditional DFT matrix generated by $O_1 = 6, N_1 = 2$ is $\{0, \pi/6, \pi/3, \ldots, 11\pi/6\}$, which does not contain $\{\pi/12, \pi/4, 5\pi/12\}$. To solve this problem, an angular offset factor $\theta_{\text{offset},u}$ is required. In this example, if we set $\theta_{\text{offset},u} = \pi/12$ and add this offset to all the angles of the traditional set, then the traditional angular set changes to $\{\pi/12, \pi/4, 5\pi/12, \ldots, 23\pi/12\}$, where the first three angles are the required angles. The operation of an angular offset is equivalent to operating the Hadamard

Table 3
Current antenna array settings in 5G.

Number of elements	Element distance	Beamwidth (°)	Total windward area (m^2)	SINR (dB)	Angle estimation accuracy ε_θ (°)	Range (m)	Localization error ε_r (m)
16	$\lambda_c/2$	6.375	0.8	15	0.5	500	9.67
16	$\lambda_c/2$	6.375	0.8	15	0.5	1000	19.32
16	$\lambda_c/2$	6.375	0.8	15	0.5	1200	23.19

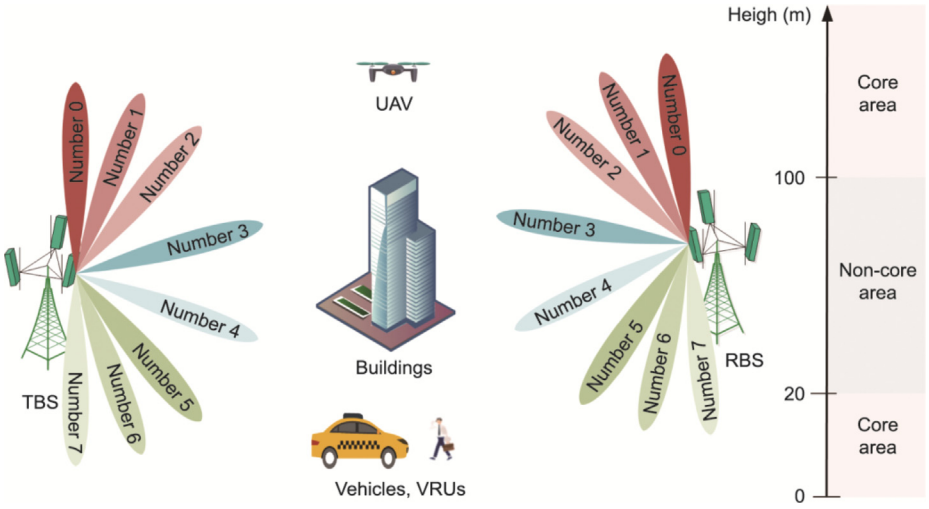

Fig. 6. Non-uniform distribution of targets in vertical space.

multiplier between the traditional DFT matrix $\boldsymbol{X}_{1,u}$ and the offset matrix $\boldsymbol{S}_{1,u}$; that is,

$$\boldsymbol{X}_{1,\text{Modified},u} = \boldsymbol{S}_{1,u} \circ \boldsymbol{X}_{1,u} \tag{12}$$

where $\boldsymbol{S}_{1,u} \in \mathbb{C}^{N_1 \times O_{1,u} N_1}$ is also a DFT-form matrix, with its pth column expressed as follows:

$$\boldsymbol{s}_{1,u,p} = \left[1, \mathrm{e}^{\frac{\mathrm{j}p\theta_{\text{offset},u}}{O_{1,u}N_1}}, \ldots, \mathrm{e}^{\frac{\mathrm{j}\theta_{\text{offset},u}p(N_1-1)}{O_{1,u}N_1}}\right]^{\mathrm{T}} \tag{13}$$

Step 3: Combine all the components of the U-modified DFT matrix $\boldsymbol{X}_{1,\text{Modified},u}$ to finally obtain the non-uniform DFT codebook matrix $\boldsymbol{X}_{1,\text{Modified}} = \left[\boldsymbol{X}_{1,\text{Modified},1}, \ldots, \boldsymbol{X}_{1,\text{Modified},U}\right]$, which corresponds to the non-uniformly distributed beam angle. The specific elements of the non-uniform DFT matrix can be expressed as

$$\boldsymbol{X}_{1,\text{Modified}} = \begin{bmatrix} 1 & 1 & \cdots & 1 \\ 1 & \mathrm{e}^{\frac{\mathrm{j}2\pi t_{1,1,1}}{O_{1,1}N_1}} & \cdots & \mathrm{e}^{\frac{\mathrm{j}2\pi t_{1,U,L_U}}{O_{1,U}N_1}} \\ \vdots & \vdots & \vdots & \vdots \\ 1 & \mathrm{e}^{\frac{\mathrm{j}2\pi(N_1-1)t_{1,1,1}}{O_{1,1}N_1}} & \cdots & \mathrm{e}^{\frac{\mathrm{j}2\pi t_{1,U,L_U}(N_1-1)}{O_{1,U}N_1}} \end{bmatrix} \tag{14}$$

where $t_{1,1,1}$ is the index of the first selected column from the first modified DFT matrix $\boldsymbol{X}_{1,\text{Modified},1}$ and t_{1,U,L_U} is the index of the last selected column from the last modified DFT matrix $\boldsymbol{X}_{1,\text{Modified},U}$.

3.2. Cluster construction

Multistatic ISAC systems utilize multiple transmit and receive nodes to perform cooperative sensing and communication. Therefore, the clusters in a multistatic ISAC system, which consist of multiple nodes that work together, can enhance the performance of both sensing and communication functionalities. By coordinating their operations, the nodes can share resources, mitigate interference, and improve the accuracy and reliability of the system. However, in cooperative sensing, it is important to select the right nodes and deploy them appropriately for enhanced performance.

3.2.1. Node selection

Node selection involves choosing the most suitable nodes from a cluster to participate in a cooperative ISAC mission. This selection process is crucial, as it determines the sensing and communication performance, resource utilization, and robustness of the overall system. Selecting the optimal cooperative nodes often involves a multi-criteria decision-making process, considering criteria such as node proximity, sensing accuracy, communication reliability, and energy efficiency. For example, consider using one Tx and K Rxs to locate one target, then for the mth Tx, gth target, the received SNR can be maximized by selecting K Rxs out of all the N Rxs, which is formulated as

$$\max_{C_k \in C_N} \sum_{c_k \in C_k} \| \boldsymbol{y}_{m,c_k,g} \|_{\mathrm{F}}^2 / \| \boldsymbol{w}_{m,c_k,g} \|_{\mathrm{F}}^2 \tag{15}$$

where C_N is the set of all the N candidate Rxs, C_k is the kth set containing K selected Rxs, and c_k represents the c_kth Rx in the set C_k. Besides, $\boldsymbol{y}_{m,c_k,g}$ and $\boldsymbol{w}_{m,c_k,g}$ are the received signal and the noise vector of the path containing the mth Tx, the gth target and the c_kth Rx, respectively.

At present, there are two prevalent node-selection strategies. The first of these strategies is proximity-based node selection, which selects the nodes closest to the transmitting node to form a cooperative cluster. Proximity-based selection prioritizes nodes near the Tx, assuming that they have stronger signal reception. However, this approach neglects the uncertainty of the target's location, which may lead to sub-optimal sensing accuracy. The second strategy is signal strength-based node selection, in which cooperative nodes are selected based on measurements such as the reference signal received power (RSRP) or the SINR. While this method accounts for signal strength, it overlooks critical environmental factors, such as interference from neighboring nodes, noise from local communication terminals, and the influences of multipath propagation and clutter.

These limitations can degrade the overall sensing performance, especially in complex network environments. To address these shortcomings, we propose an advanced node-selection strategy that leverages the SINR of each path (SINR-P) as a key metric. The SINR-P considers real path loss and interference, providing a more comprehensive and accurate measure for cooperative node selection. The proposed method operates as shown in Fig. 7. TBS A initiates sensing through wide-beam detection, transmitting signals that are reflected by the target and received by neighboring RBSs (i.e., B, C, and D). Each neighboring RBS reports the SINR-P of the first path farther than the direct path or the first path with a non-zero velocity. TBS A then compares the SINR-P values to determine optimal cooperative nodes (e.g., RBS B) for further sensing.

By integrating SINR-P metrics with periodic measurements, the proposed method significantly enhances the performance of

cooperative sensing systems compared with traditional approaches. It increases accuracy by considering real path loss, interference, and dynamic network conditions, while offering flexibility through the dynamic adjustment of cooperative nodes based on real-time network changes. Additionally, the proposed method increases robustness by mitigating the effects of target location uncertainty and environmental interference.

3.2.2. Node deployment

The spatial distribution of nodes directly influences the system's ability to achieve accurate sensing and reliable communication. When deploying nodes, it is thus necessary to consider the overall network topology, ensuring that nodes are strategically placed to maximize coverage and minimize interference. Factors such as the number of nodes, their positions, and the communication links between them all play a crucial role in determining the system's performance. To meet both sensing and communication requirements, adequate signal strength and quality for both tasks is another important factor to consider. Moreover, the deployment should be scalable, allowing for the addition of new nodes as needed to expand the network's capabilities. It should also be flexible, enabling the system to adapt to changes in the environment or mission requirements.

Optimal node deployment ensures that the system can cover the desired area with minimal redundancy and interference, thereby maximizing efficiency [53]. Grid-based deployment is a deployment strategy in which nodes are arranged in a predefined pattern to provide uniform coverage and ease of management. An example involving Rx node deployment in a BS cell is shown in Fig. 8. In the figure, red diamonds mark the optimal node deployment, while blue circles refer to the uniform distribution of the receiving nodes. For an optimal distribution, the receiving nodes should be densely distributed at the edge of the cell but distributed with lower density when close to the BS. However, this approach may not be feasible in environments with irregular topographies or dynamic conditions. Alternatively, random deployment, in which nodes are scattered over the area of interest without any predefined pattern, offers greater flexibility. This strategy is particularly suitable for large-scale networks where manual placement is impractical and movable sensing nodes are used. However, random deployment can lead to uneven coverage and potential communication bottlenecks. Fig. 9 shows a comparison of these two strategies, the worst SINR can be improved by 7 dB through optimization. To address these challenges, adaptive deployment strategies have emerged as a promising solution. These strategies utilize real-time data and feedback to dynamically adjust the node positions, ensuring optimal coverage and performance. Machine learning and artificial intelligence (AI) algorithms

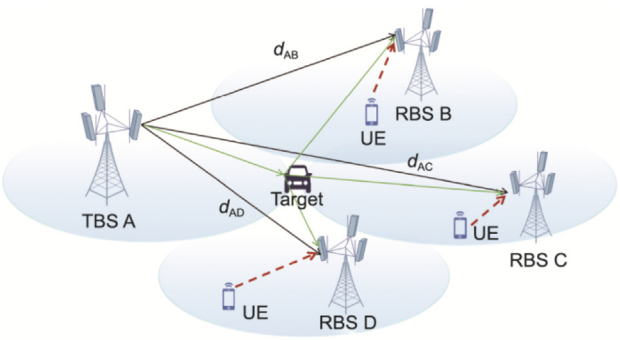

Fig. 7. TBS A determines a cooperative node. d_{AB}, d_{AC}, and d_{AD}: the distance from TBS A to RBS B, RBS C, and RBS D, respectively.

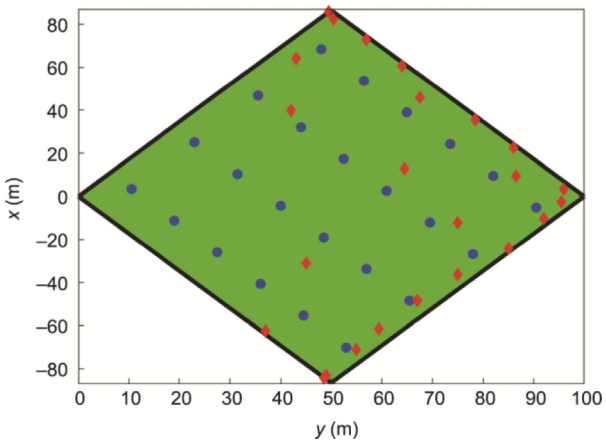

Fig. 8. Deployment of receiving nodes within a BS cell. x and y: the x-coordinates and y-coordinates of the receiving nodes, respectively.

can be employed to predict and optimize node placement based on environmental conditions and system requirements.

3.3. Synchronization

In a cooperative ISAC system, synchronization is a fundamental requirement that ensures that the data collected by different nodes is consistent and can be accurately correlated [68]. For example, a 65 ns synchronization error in 5G will cause a 20 m sensing ranging error, demonstrating that synchronization is very important for sensing performance.

3.3.1. Timing synchronization

To solve the inter-node synchronization problem, we propose two air–interface calibration methods: the round-trip measurement-based method and the reference path-based method (Fig. 10). The round-trip method eliminates the timing error by transmitting the sensing signals from TBS A to RBS B, then from RBS B to TBS A. The reference path-based method is described as follows. Measuring the LoS path delay between the Tx and Rx is a straightforward way to obtain the time difference; as long as the positions of the Tx and Rx are known, the difference between the measured delay and the ideal delay can be eliminated in the sensing results to achieve timing synchronization. The timing difference Δt is given by

$$\Delta t = T_{\text{mea}} - \frac{d_{\text{los}}}{c} \tag{16}$$

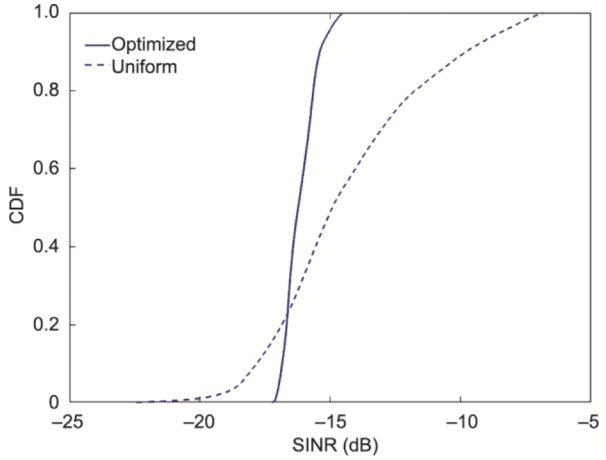

Fig. 9. Node-selection optimization results. CDF: cumulative distribution function.

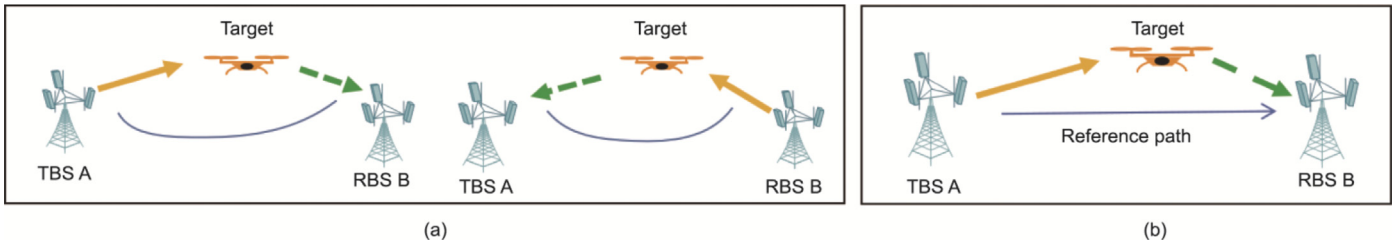

Fig. 10. Schematic diagram of the two synchronization methods. (a) Round-trip transmitting and receiving measurements; (b) reference path-based measurements.

where T_{mea} is the measure path delay and d_{los} is the distance of the LoS connecting the TBS A and RBS B. When the LoS path is blocked, we can use a known scatter to form a reference path.

3.3.2. Frequency synchronization

Frequency synchronization ensures that all devices within a network are operating on the same frequency channels, as frequency offsets can lead to degradation in velocity estimation accuracy in the sensing process. The LTE standard includes a frequency synchronization mechanism that allows BSs to synchronize their clocks and frequencies using the signals transmitted by a central node. Another solution is to use distributed frequency synchronization algorithms. These algorithms allow nodes to iteratively adjust their frequencies by exchanging timing and frequency information with their neighbors. One example of a distributed frequency synchronization algorithm is the flooding frequency synchronization protocol (FFSP), which uses message exchanges between nodes to estimate and correct frequency offsets. In addition to these algorithmic solutions, advancements in hardware can help address frequency synchronization challenges. For example, the use of high-precision oscillators and frequency-locked loops (FLLs) can improve the accuracy of a node's frequency.

Similarly, the use of an LoS path based on reference path measurements works for frequency synchronization where the measured Doppler frequency is exactly the same as the asynchronization value, since the ideal value is zero for an LoS path. Using the LoS path to compensate for both the timing and the frequency asynchronization can greatly improve estimations of the distance and velocity of the object, as shown in Fig. 11. A synchronization trial is further described in Section 6.1.

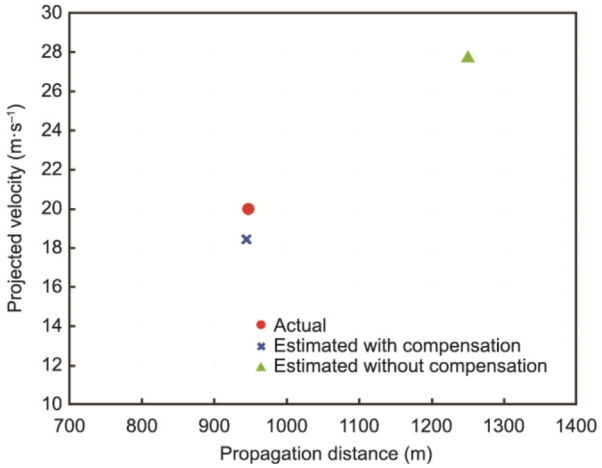

Fig. 11. Distance and velocity estimation with and without timing and frequency synchronization.

3.4. Data fusion

Data fusion in ISAC refers to the process of combining, integrating, and interpreting data from multiple sensors or communication systems to produce more accurate, reliable, and comprehensive information. This process involves the application of algorithms, processes, and protocols that enable the extraction of valuable insights from raw data, thereby improving the system's performance and decision-making capabilities [69]. There are three levels of data fusion, as shown in Fig. 12.

3.4.1. Signal-level data fusion

The core principle of signal-level data fusion is its ability to integrate raw signals from multiple sources at the earliest possible stage of processing. This early integration ensures that the maximum amount of information is preserved and utilized, leading to more accurate and comprehensive sensing and communication outcomes. To perform signal-level data fusion, each Rx sends the original received sensing signal to the sensing server. The server then performs data fusion to combine all the signal results. This method requires the lowest signal-processing capability from the Rxs, while a large amount of data needs to be sent, occupying too many resources for data transmission. For the server, this data fusion process is extremely complex, since a large quantity of signals must be dealt with, significantly slowing down the output of sensing results.

3.4.2. Symbol-level data fusion

Symbol-level data fusion has a higher level of abstraction than signal-level data fusion but still retains crucial information for accurate sensing. During this process, each node may capture different aspects of the environment or target containing multiple points, such as the range, angle of arrival, velocity, or position. These aspects are then sent to the sensing server, where this

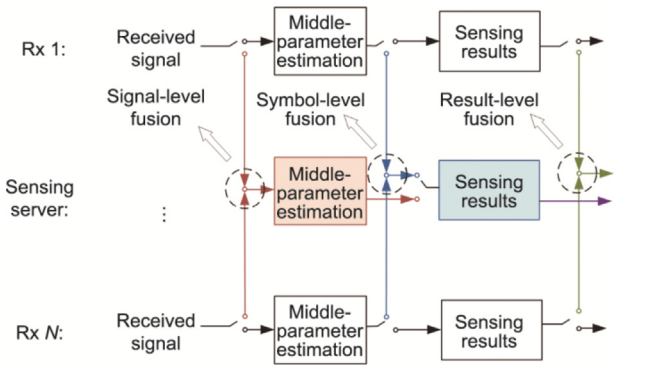

Fig. 12. Block diagram of the three levels of data fusion: signal-level fusion, symbol-level fusion, and result-level fusion.

diverse data is integrated to obtain the shape, trajectory or the centroid position of the sensing targets. The symbol-level data fusion is particularly important in complex environments, where a single Rx may be insufficient to capture all relevant information. In this method, the signal-processing complexity for the Rx and sensing server is balanced, and significantly fewer resources are required for data transmission in comparison with those needed for signal-level data fusion.

3.4.3. Result-level data fusion

Result-level data fusion involves the aggregation and analysis of data at the final stage of processing, after individual Rxs have generated their own results. One of the key methodologies for result-level data fusion is decision-making, which analyzes the results generated by each node, identifies inconsistencies and redundancies, and combines this information to create a more accurate and reliable representation of the sensed environment or target. Techniques such as majority voting, weighted averaging, and Bayesian networks are commonly employed to achieve this goal. Although this data-fusion level requires the least amount of information to be transmitted, the sensing accuracy is the worst among the three levels, due to signal compression and quantization in signal processing.

Fig. 13 illustrates the positioning accuracy of the three data-fusion methods. It can be observed that each method exhibits unique characteristics in terms of balancing the trade-off between signal-processing complexity and sensing performance. In particular, symbol-level data fusion method provides a compromise in this regard, as it maintains high localization accuracy without unnecessarily burdening signal-processing resources.

In contrast, other fusion approaches may either demand excessive computational power and complexity, potentially leading to higher latency and energy consumption, or compromise on the precision of positioning data, which is critical for many ISAC network applications. Therefore, when considering the practical implementation of ISAC networks, where both accurate sensing and efficient communication are paramount, the symbol-level data-fusion method emerges as the more desirable option.

3.5. Interference management and networking

In Section 3.3, node deployment was investigated, although this task is not associated with current cellular network topologies. For the purpose of reusing current cellular networks to achieve cooperative sensing, it is necessary to determine which site or cell will be the sensing Tx and which will be the Rx. If the layout is not properly designed, interference issues will occur. Therefore, the key technologies of interference management and networking are tightly related.

In this subsection, we propose a networking scheme for cooperative sensing while considering interference mitigation, and give guidance on how to set up a combination of multiple cells to provide service to targets located within a certain cell. An urban macro (UMa) scenario with 19 sites is considered, as shown in Fig. 14. Each site contains three cells, for a total of 57 cells. The cells have indices of {1, 2,. . ., 57}, where the qth site contains the cells with the indices $\{(3q-2), (3q-1), 3q\}$.

In terms of networking, two types of interference must be considered: inter-cell/intra-site interference and inter-site interference. Inter-cell interference in cooperative sensing can be solved by setting all three cells in the same site to be sensing Txs or Rxs [70]. That is, the working slots of the three cells within one site should all be either downlink or uplink. To mitigate inter-site interference (which is usually strong between neighboring sites), the sensing Txs and Rxs must be spatially separated. To achieve this, we propose a ring-shaped networking scheme for cooperative sensing. Transmitting and receiving cells are arranged in concentric rings, alternating between transmitting and receiving layers from the center outward. In Fig. 14, the transmitting cells are colored green and the receiving cells are grey. This configuration ensures physical isolation between Txs and Rxs while optimizing coverage. The specific rings and corresponding sites are listed in Table 4. In this way, the number of interference cells for cell 5, for example, decreases from 56 to 20.

Based on the proposed ring-shaped networking scheme, there are two options to divide the sensing areas. One option is cell-centric, in which the transmitting cell and the four receiving cells

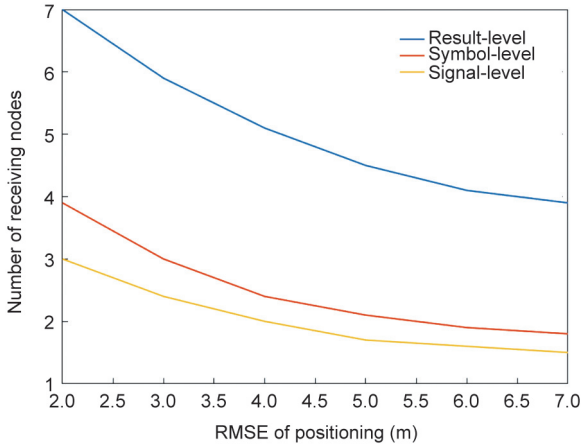

Fig. 13. Positioning accuracy of the three data-fusion levels. RMSE: root mean squared error.

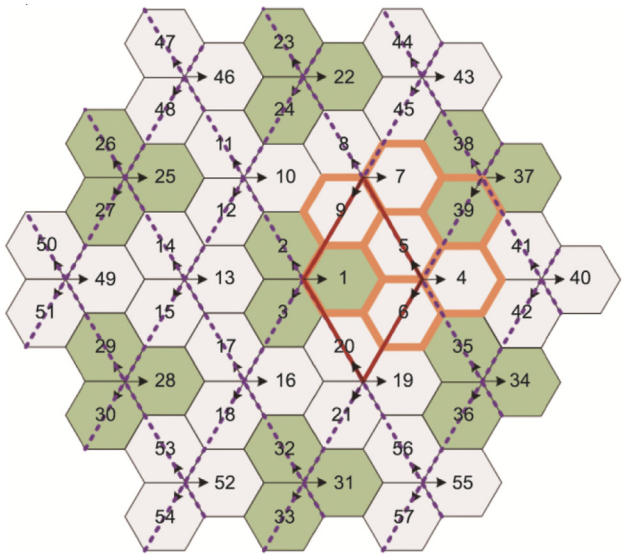

Fig. 14. Ring-shaped networking scheme for cooperative sensing.

Table 4
Rings and corresponding sites in the ring-shaped networking for cellular networks shown in Fig. 14.

Function	Ring	Number of sites	Site indices
Sensing Txs	Inner	1	1
	Outer	6	8, 9, 10, 11, 12, 13
Sensing Rxs	Inner	6	2, 3, 4, 5, 6, 7
	Outer	6	14, 15, 16, 17, 18, 19

it points to are combined to provide sensing service for targets within their area. To equally distribute each cluster, their areas are set to be diamond-shaped, as divided by the purple dashed line in Fig. 14. The other option is target-centric, in which all the cells around the target form a sensing cluster. For example, as shown by the orange line in Fig. 14, for the targets in cell 5, cells 1 and 39 are arranged to be the Txs and cells 4, 5, 6, 7, and 9 are the Rxs. In this way, the sensing accuracy can be ensured.

4. Key performance indicators

Defining KPIs is vital for technical solution development and system design and will establish a clear framework for evaluating and optimizing system performance and promoting standardization across different scenarios. By quantifying trade-offs and standardizing performance benchmarks, well-defined KPIs will enable a high-quality, efficient, and scalable ISAC network. For traditional radar systems, performance metrics such as range accuracy and missed detection rate have been defined. The communication KPIs that have been defined in previous generations such as 4G and 5G includes data rate, spectral efficiency, throughput, latency, mobility, and other metrics.

When defining KPIs for ISAC, both communication and sensing aspects should be considered. Concepts from the field of radar can be borrowed to demonstrate the performance of the novel sensing capabilities of 6G. In addition to considering radar KPIs, it is necessary to balance the needs of communication in defining ISAC requirements. Below, we define the KPIs for 6G ISAC and provide suggestions for performance evaluation and KPI values.

4.1. Current sensing metrics

Detection and estimation are two of the main radar operations, each of which has its corresponding metrics. The detection probability is the probability of correctly detecting the presence of the object, and the false alarm probability is the probability that an object will be detected even though no object is present. These metrics are critical for ensuring the reliability of detection tasks. A high detection probability is essential to accurately identify targets in various applications, including safety–critical scenarios such as UAV tracking; at the same time, minimizing the false alarm probability is crucial to reduce unnecessary interventions and maintain operational trust. A trade-off must be maintained between these two metrics. When conducting target detection, if the detection threshold is high, then fewer peaks (corresponding to detectable objects) will be detected. The false alarm probability will be low, but the detection probability will also decrease.

Estimation accuracy is defined as the difference between the measured magnitude and the actual magnitude of sensed objects; it is applied to various measurements such as the range, angle, location, and velocity. Accuracy is normally recorded in terms of a confidence level, which refers to the degree of certainty or reliability that a sensing system's measurements are correct. The sensing accuracy can be obtained from the cumulative distribution function (CDF) plot of sensing estimation error, with typical confidence level values of 80% or 90%. In addition, the bound of estimation accuracy is usually used in theoretical analysis, where the most typical is the Cramér Rao lower bound (CRLB).

The sensing KPIs mentioned above have the following shortcomings, which should be addressed to adapt the KPIs to 6G cooperative ISAC systems:

(1) Current sensing KPIs are defined for radar-only systems, which do not consider the coexistence of communication. The coexistence of sensing and communication introduces resource competition between these two functionalities. As a result, the sensing performance will be constrained in many circumstances due to resource limitations. Therefore, the sensing KPIs should define achievable performance under restricted resources.

(2) Current sensing KPIs are mainly single metrics, where "single" refers to three aspects: a single node or cluster, single KPI, and single target. Regarding a single node or cluster, current KPIs mainly have required values for monostatic or bistatic sensing topologies, and there is usually no required KPI value for multistatic topologies. Regarding a single KPI, detection and estimation metrics are defined separately, while their interaction is not considered. Regarding a single target, current KPIs mainly focus on a specific target; however, with the development of sensing applications such as UAVs and V2X, there are usually multiple targets within a sensing area. Therefore, the interaction between targets should be considered. Also, it is necessary to answer the question of how many targets can be served simultaneously, which directly reflects the sensing capability of the ISAC system. However, KPIs corresponding to this question are absent in current KPI frameworks.

4.2. Network sensing capacity

To solve the shortcomings of the current sensing KPIs mentioned above, in this subsection, we propose the use of sensing capacity as a metric to reflect the system-level performance of a sensing system. Sensing capacity is defined as the number of targets per square kilometer that fulfill sensing quality-of-service (QoS) requirements [64]. This metric is crucial for ensuring the scalability and effectiveness of sensing systems in complex, dynamic environments, such as UAV detection and tracking, autonomous vehicles, and industrial automation. High sensing capacity allows for broader coverage and efficient resource utilization, enabling systems to handle increasing operational demands while maintaining accuracy and efficiency.

The abovementioned sensing QoS requirements include localization accuracy and sensing latency. A trade-off exists between the localization accuracy and the air–interface sensing latency in an ISAC system. On the one hand, a very long sensing latency will jeopardize the communication performance. On the other hand, a high sensing latency indicates multiple sensing signal transmissions for a higher signal-to-noise ratio (SNR), which leads to better localization accuracy.

5. Performance evaluation

In this section, we focus on the performance evaluation of UAV detection, which is an emerging scenario. We demonstrate an evaluation methodology and present simulation results and expected KPI values. For the performance indicators of interest, we concentrate on detection probability for a given false alarm probability and on sensing capacity, as localization accuracy is part of the sensing QoS requirements within the definition of sensing capacity.

5.1. Evaluation methodologies

The evaluation methodology for detection probability is as follows:

(1) Perform a system-level simulation and initialize the evaluation parameters with a chosen false alarm probability.

(2) Generate a sensing transmit signal and obtain the received signal. Perform sensing signal processing and record whether a sensing object is detected or not.

(3) Repeat steps 1 and 2 for a total number of G targets and record the number of successfully detected targets, denoted as S_{dect}.

(4) Calculate the detection probability (P_{dect}) as $P_{\text{dect}} = S_{\text{dect}}/G$.

The evaluation methodology for sensing capacity is as follows:

(1) Perform a system-level simulation and initialize the evaluation parameters with a chosen sensing latency.

(2) Generate a sensing transmit signal and obtain the received signal. Perform sensing signal processing to obtain the localization estimation error for each sensing target.

(3) Plot the CDF of the localization estimation error and record the portion (P) of sensing objects that fulfill the given localization accuracy requirement.

(4) Calculate the sensing capacity (C) as $C = GP/A$, where A is the area of the sensing network layout.

5.2. Evaluation assumptions

In this section, Table 5 provides the parameters used for the simulation and Fig. 14 shows the network layout. For the evaluation of detection probability, we use a mono-static sensing mode (i.e., the sensing Rx and Tx are the same device) to ensure the reliability of the detection results. For the evaluation of sensing capacity, we consider a multistatic sensing system with cell 1 as the Tx and cells 5, 6, 9, and 20 as the Rxs, as shown in Fig. 14.

5.3. Simulation results

In this subsection, we present the simulation results and provide suggestions for the KPI value accordingly. Fig. 15 demonstrates the detection probability results for different false alarm probabilities. The detection probability performance worsens as the false alarm probability requirements get stricter, which is in line with the discussion in Section 4.1. The suggested KPI for detection probability is 95% for a false alarm probability of 10^{-6}; other requirements for different false alarm probabilities can also be set.

Fig. 16 demonstrates the performance gain of the designed ring-shaped networking scheme, in comparison with that of a non-cooperative sensing networking scheme named "fish scale," where each site mutes two cells when using the remaining cell to simultaneously transmit and receive sensing signals, as introduced in Ref. [70]. Cooperative sensing can conduct energy accumulation by collecting the sensing signals of different cells, while non-cooperative sensing cannot. Considering the sensing area outlined with red in Fig. 14, when the target is 100, 200, or 300 m away from the sensing sites, the proportion of accumulating energy twice or more (with the RSRP difference of the sensing channel within 6 dB) reaches over 80% for cooperative sensing. Moreover, the energy accumulation of cooperative sensing is about 25 dB higher than that of non-cooperative sensing.

6. Field trial

Synchronization among nodes is a fundamental requirement for cooperative sensing, as it directly influences the consistency and accuracy of data integration across the network. By aligning the timing of data collection from multiple nodes, synchronization ensures seamless information fusion, forming the foundation for effective collaboration. Validating the effectiveness of synchronization technology is, therefore, a critical step to address potential temporal inconsistencies within the system. Once reliable synchronization is established, the next key task is to investigate its impact on the overall sensing performance of the cooperative network. This step is motivated by the need to quantify how improved synchronization enhances system capabilities such as sensing accuracy and data fusion reliability. To achieve these objectives, we conduct a two-phase experimental evaluation: first, by assessing the performance and robustness of the synchronization technology itself; and, second, by analyzing the sensing performance improvements achieved after synchronization is implemented.

In this section, we present the experimental results for the synchronization method and sensing performance. A high-frequency system is utilized to validate the effectiveness of the synchronization technology, while a low-frequency system is employed to evaluate the sensing performance after synchronization has been achieved.

Table 5
Simulation parameters.

Parameter	Value
Carrier frequency for evaluation (GHz)	7
Bandwidth (MHz)	100
Subcarrier spacing (kHz)	30
UAV RCS (m^2)	0.1
Number of horizontal antennas	8
Number of vertical antennas	16
Polarization number	2
BS antenna element gain (dBi)	8
BS noise figure (dB)	5
Inter-site distance (m)	200
BS antenna height (m)	25
Transmit power per BS (dBm)	52

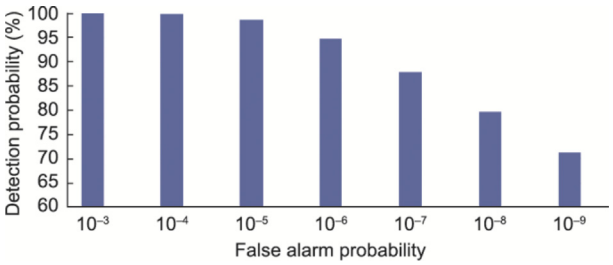

Fig. 15. Simulation results of detection probability for different false alarm probabilities.

6.1. Synchronization validation

To address the multi-node synchronization challenge in cooperative sensing, we propose a synchronization scheme based on air–interface calibration and use a high-frequency millimeter-wave prototype to validate various synchronization solutions, including the air–interface calibration and direct fiber connection. In this subsection, we first introduce the prototype design and parameters and describe the test scenarios for the high-frequency experiment, followed by the experimental results for both sensing and communication functions.

6.1.1. High-frequency ISAC prototype design and parameters

A millimeter-wave baseband prototype was designed to process received OFDM signals through a series of steps, including signal sampling, demodulation, and digital signal processing (DSP). The system begins by capturing incoming millimeter-wave signals using high-speed analog-to-digital converters (ADCs), ensuring accurate sampling of the received OFDM waveforms. The sampled signals are then fed into the OFDM demodulation module, where they undergo fast Fourier transform to extract the frequency-domain subcarriers. Channel estimation and equalization techniques are applied to ensure robust signal recovery. Subsequently, the system performs DSP operations to retrieve the target information with high accuracy.

The configuration parameters for the trial are provided in Table 6.

6.1.2. High-frequency ISAC test scenario

The synchronization scheme verification setup is depicted in Fig. 17. The prototype consists of a Tx, Rx, UE, and processing unit.

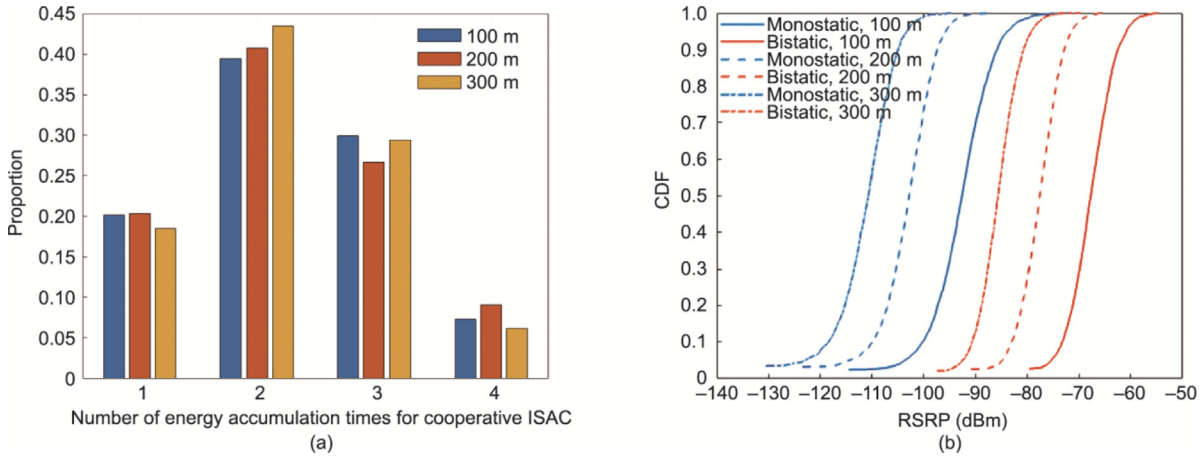

Fig. 16. Comparison of the energy accumulation ability of cooperative versus non-cooperative sensing: (a) energy accumulation times and (b) RSRP.

Table 6
Configuration parameters of the prototype.

Parameter	Value
Center frequency (GHz)	26
Bandwidth (MHz)	200
Number of antennas	256
Equivalent isotropic radiated power (dBm)	58
Waveform	OFDM
Scheme and sensing resource	Time-division, 1/28

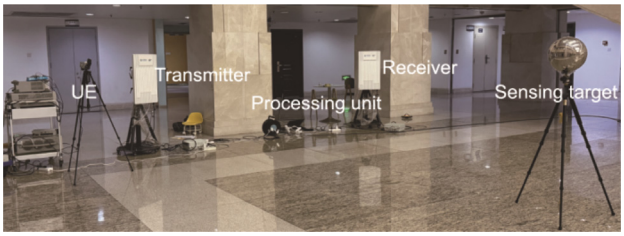

Fig. 17. Setup of the high-frequency ISAC prototype trial scenario.

The Tx supports a large bandwidth and multi-antenna capabilities, and is used to transmit both communication and sensing signals. The Rx receives the echo signals reflected by the target, and the processing unit analyzes and processes the echo signals based on various synchronization techniques to obtain the target sensing information. The communication signal is received by the UE, which measures the transmission rate.

6.1.3. Sensing results

To evaluate the performance of two synchronization schemes, a series of experiments were conducted within a test range of 4–6 m. Multiple target points were selected within this range to assess both synchronization accuracy and distance performance. First, the synchronization schemes were applied to achieve synchronization between the two nodes. After synchronization, the distance estimations for each target point were measured, and the corresponding distance errors were calculated. The CDF curves of the distance errors obtained from multiple trials are shown in Fig. 18(a). The results demonstrate that the fiber direct connection scheme outperforms the air–interface calibration scheme in terms of distance error. Additionally, both schemes are capable of achieving a distance accuracy under 0.5 m.

In the statistical analysis of the test trials, the distance accuracy for the fiber direct connection scheme was 0.1556 m, while the air–interface calibration scheme achieved a distance accuracy of 0.1941 m. These results highlight the effectiveness of both synchronization techniques and provide a solid experimental foundation for the verification of key technologies in cooperative sensing.

6.1.4. Communication results

In parallel with the synchronization and sensing performance evaluation, communication testing was also conducted during the experiment. A horn antenna was used as the UE to receive and process the communication signals. Within a communication range of approximately 1 m, the system utilized 16-quadrature amplitude modulation (QAM) to transmit a data stream, achieving a transmission rate of 683.78 megabits per second (Mbps) without the overhead of pilot signals. The communication signal performance was assessed based on the received constellation diagram, as shown in Fig. 18(b). It can be seen that the horn antenna successfully demodulated the transmitted symbols from the received signal, demonstrating reliable signal reception.

The test results show that the prototype was able to transmit communication data in real time while achieving decimeter-level ranging accuracy. Through this test, we not only validated the feasibility of the synchronization technology solutions but also provided an important reference for future 6G ISAC applications.

Observation 1: The synchronization technology enables effective cooperative sensing. The experimental results demonstrate that synchronization between nodes can be achieved effectively through advanced techniques such as air–interface calibration and fiber direct connection. These methods provide a solid foundation for cooperative sensing, ensuring sub-meter-level distance accuracy and reliable synchronization even in complex environments.

6.2. Performance evaluation for bistatic ISAC

In this subsection, we evaluate the sensing performance of a bistatic ISAC system after the implementation of synchronization technology. We first introduce the prototype design and parameters, as well as the test scenario for the low-frequency bistatic experiment, followed by the experimental results for sensing functions.

6.2.1. Low-frequency bistatic ISAC prototype design and test scenario

This subsection describes the sensing test, which was conducted collaboratively by two sites, denoted as site 1 and site 2,

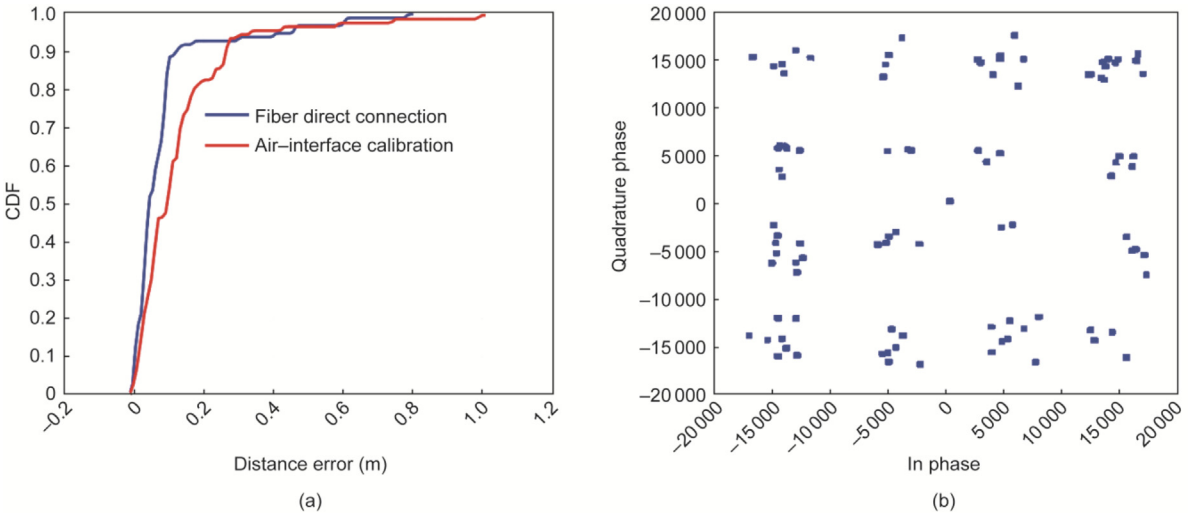

Fig. 18. Results from the high-frequency ISAC prototype trial: (a) sensing results and (b) communication results.

with each site deploying a 4.9 GHz ISAC active antenna unit (AAU) mounted at a height of approximately 75 m. Each site was equipped with a total of 64 Tx and Rx antennas, with a 192-element antenna array and a mechanical tilt of 20°. The distance between the two nodes was 800 m. The main objective was to apply synchronization technology based on existing low-frequency BSs to achieve sensing functionality.

The trial was conducted in a typical urban area, with the presence of static clutter sources such as mountains, as well as dynamic clutter from pedestrians and vehicles. Airborne targets such as flying birds and low-flying aircraft could also interfere with the sensing system.

Transmission and reception were directed toward the center of the coverage area, forming an elliptical sensing region. The two sites were synchronized via air–interface calibration. A UAV equipped with a real-time kinematic (RTK) positioning system was used for the sensing tests, verifying KPIs such as coverage range, sensing accuracy, false alarm probability, missed detection rate, and resolution. The UAV followed a specific flight trajectory, taking off or landing from random positions within the coverage area and flying in a grid-like pattern, with intersecting straight lines spaced 200 m apart. The UAV's trajectory is depicted in Fig. 19.

6.2.2. Sensing performance

(1) **Sensing coverage.** To assess the sensing coverage, the UAV was flown at different altitudes to test the sensing distance. The CDF of the sensing distance at various altitudes of 100, 200, 300, and 375 m is shown in Fig. 20(a). The data indicates that the cooperative sensing range of the two stations covers more than 700 m.

(2) **Sensing accuracy.** The CDF results for horizontal and vertical accuracy are shown in Fig. 20(b). The testing results indicate that, at a 95% confidence level, the horizontal accuracy is 6.41 m, and the vertical accuracy is 10.24 m. These accuracy results demonstrate that the system can provide sufficiently accurate target location estimates, meeting the needs of low-altitude economic applications.

(3) **False alarm and missed detection rates.** In the no-target scenario, a long-duration target-detection test was conducted, with the results showing a no-target false alarm probability of 3.5%. In scenarios with detected targets, a long-duration test revealed some missed detections. The missed detection rate was found to be 3.6%, indicating that the system's overall false alarm and missed detection rates are within an acceptable range.

(4) **Sensing resolution.** A far-distance test with two targets was conducted to verify the system's minimum sensing distance, which was determined to be 3.06 m. This result indicates that the system can accurately detect targets that are less than 3 m apart, demonstrating good resolution capabilities.

This test validated the performance of the bistatic cooperative sensing system in a real-world environment. By employing the air–interface calibration synchronization scheme, the system was able to achieve target sensing even in a complex urban environment. The results show that the system's coverage range, accuracy, false alarm probability, and missed detection rate are within acceptable limits for low-altitude economic applications. Further tests in more complex environments are recommended to continue evaluating and improving the system's robustness and reliability.

Observation 2: Bistatic cooperative sensing meets the requirements for low-altitude economic applications. The bistatic cooperative sensing system offers superior performance in terms of coverage range, accuracy, resolution, and false alarm probability. The system achieves a coverage range of 700 m, horizontal accuracy of 6.41 m, vertical accuracy of 10.24 m, and

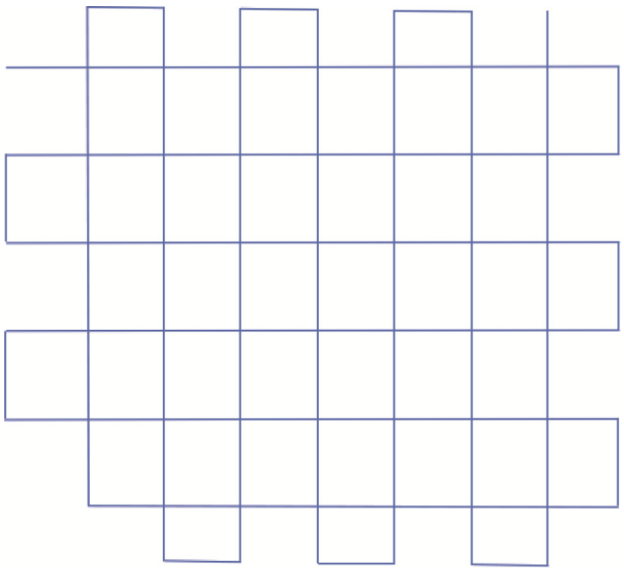

Fig. 19. UAV trajectory in the prototype trials.

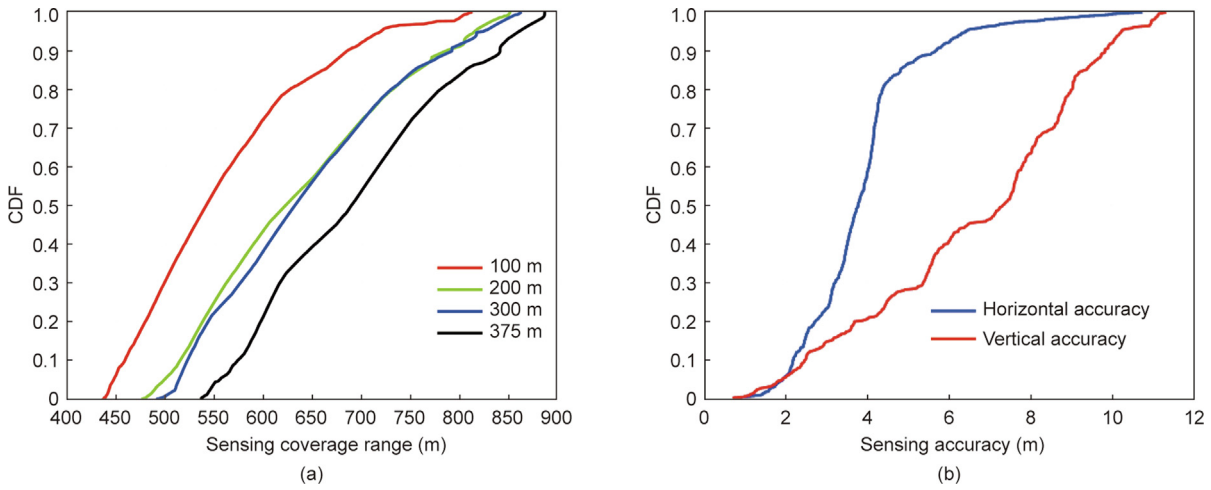

Fig. 20. Results for the low-frequency bistatic ISAC prototype trial: (a) sensing coverage range and (b) sensing accuracy.

resolution of 3.06 m, meeting the requirements for low-altitude economic applications.

6.3. Performance evaluation for multistatic ISAC

In this subsection, we evaluate the sensing performance of a multistatic ISAC system after implementation of the synchronization technology. We first introduce the prototype design and parameters, as well as the test scenario for the low-frequency multistatic experiment, followed by the experimental results for sensing functions.

6.3.1. Low-frequency multistatic ISAC prototype design and test scenario

The sensing test was collaboratively conducted by three sites, each equipped with a 4.9 GHz ISAC AAU mounted at a height of approximately 50 m. Each site was configured with 64 Tx or 64 Rx antennas, utilizing a 192-element antenna array with a mechanical tilt of 0°. The main objective was to apply the synchronization technology based on existing low-frequency BSs to evaluate the multistatic sensing functionality. The UAV settings in this test were the same as those in the bistatic test.

In the real-world outdoor test, a three-node configuration was implemented, with distances between the sets of two nodes of 860, 960, and 980 m. The transmission and reception were directed toward the center of the coverage area. The test area was located in a densely populated urban environment. In this scenario, the three sites were synchronized using air–interface calibration.

6.3.2. Sensing performance

Through sensing tests on UAV targets, we obtained the sensing performance of the three-station cooperative sensing system. Using a grid-like flight trajectory, we verified that the sensing coverage requirements among the three stations could generally be met. Table 7 presents the test results for horizontal accuracy, vertical accuracy, false alarm probability, and missed detection rate at different altitudes. The results indicate that the accuracy is within 20 m, meeting the 20 m positioning requirements, while the false alarm probability and missed detection rate remain within acceptable ranges. In addition, we conducted a dual-UAV flight test to verify the system's resolution capability. The results showed that the system could still detect and distinguish between two UAVs with a separation distance of 10 m.

This test validated the performance of the three-station cooperative sensing system. The results show that the system's coverage range, accuracy, false alarm probability, and missed detection rate are within acceptable limits for low-altitude economic applications.

Observation 3: Multistatic cooperative sensing further enhances performance. By addressing blind spots and improving the overall sensing performance, the multistatic cooperative sensing system demonstrates significant advantages in coverage and accuracy. The three-node configuration achieves an average coverage distance of 900 m, with a positioning accuracy of under 20 m and the ability to distinguish targets as close as 10 m apart. This highlights its scalability and suitability for large-scale and dense urban deployment scenarios.

6.4. Performance evaluation for networked ISAC

In this subsection, we evaluate the sensing performance of the networked ISAC system after implementing synchronization technology. The experimental setup and results are described below.

6.4.1. Low-frequency network ISAC prototype design and test scenario

The field trial used a configuration of 13 sites with an average inter-site distance of 770 m. Each site was equipped with a 4.9 GHz ISAC AAU mounted at a height of about 50 m and deployed in a densely populated urban core area. The specific test setup is illustrated in Fig. 21(a). The test environment included diverse scenarios, such as residential zones, government buildings, commercial complexes, and parks, with over ten high-rise structures

Table 7
Sensing performance in low-frequency multistatic ISAC prototype trial.

Flight altitude (m)	Horizontal accuracy (CDF 95%) (m)	Vertical accuracy (CDF 95%) (m)	False alarm probability (%)	Missed detection probability at 20 m accuracy (%)
100	14.90	8.14	4.72	3.51
200	11.74	7.53	4.72	3.51

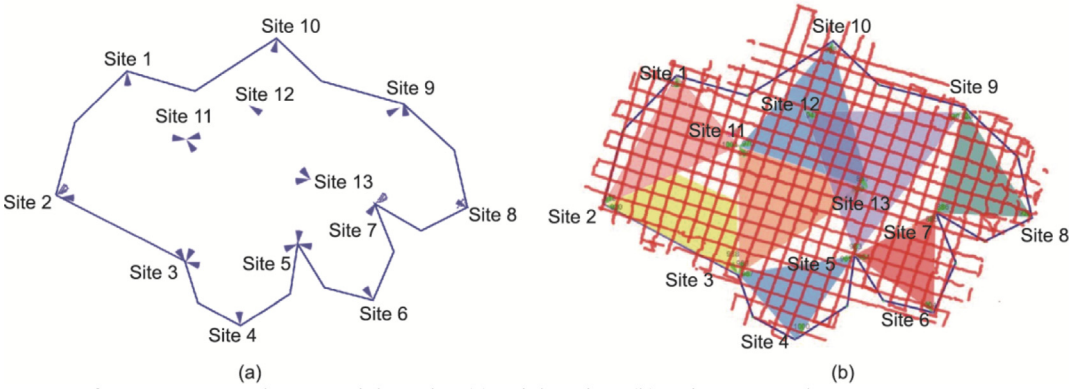

Fig. 21. Low-frequency network ISAC trial results: (a) trial setting and (b) trajectory results.

exceeding 60 m in height. This setup aligns with typical urban characteristics and validates the system's adaptability to complex topographies.

6.4.2. Sensing performance

We evaluated the cooperative sensing performance using UAV targets with RTK positioning. A grid-like flight trajectory was used to test coverage and sensing accuracy. The test results showed that a positioning accuracy of 14 m was achieved in the 100–300 m altitude range, significantly exceeding the 20 m requirement. The false alarm probability was 3% and the missed detection rate was 3.2%, which meet the requirements for low-altitude economic applications. The trajectory results shown in Fig. 21(b) further confirm the system's ability to maintain seamless coverage while utilizing a shared spectrum and hardware resources. These results highlight the potential of a networked ISAC system for urban air traffic.

This test validates the performance of the cooperative sensing system in large-scale cellular networks. The results show that the system's coverage, accuracy, false alarm probability, and missed detection rate are all within acceptable limits for low-altitude economic applications.

7. Future research directions

The following research directions are suggested for further investigation:

(1) **AI-driven signal processing and optimization.** AI is poised to revolutionize cooperative sensing for 6G ISAC. Advanced AI models—particularly deep learning and reinforcement learning—can significantly enhance signal processing capabilities. AI-driven optimization algorithms can dynamically adapt beamforming, power allocation, and resource scheduling to improve sensing accuracy and robustness in dynamic environments.

(2) **AI-augmented sensing with semantic information.** Semantic sensing leverages AI to extract high-level features from raw data, such as object identification, behavior prediction, and environmental mapping. This enables a deeper integration of sensing with intelligent decision-making processes, transforming cooperative sensing into a context-aware system. For cooperative sensing specifically, semantic information can optimize multi-node operations by increasing the contextual understanding of sensed data. For instance, AI can infer motion patterns or identify anomalies across multiple sensing nodes, improving synchronization and data fusion efficiency. Additionally, semantic augmentation reduces data transmission overhead by focusing on high-level insights rather than raw data, which is particularly valuable in bandwidth-constrained cooperative networks.

(3) **Agent-based systems in cooperative sensing.** Agent-based systems introduce autonomous decision-making capabilities into cooperative sensing. Each node, or agent, operates with a degree of autonomy, making localized decisions based on environmental inputs while adhering to global coordination protocols. This approach reduces the latency of centralized control and increases adaptability in dynamic environments. Agents can dynamically form or dissolve cooperative clusters based on task requirements, resource availability, and environmental changes, ensuring optimal utilization of the network. Furthermore, integrating AI-driven agents enables predictive analytics, such as preemptive fault detection and adaptive load balancing, significantly increasing the overall efficiency and resilience of the cooperative sensing framework. Cooperative sensing systems can achieve superior spatial and temporal resolution by integrating data from multiple stations and angles. This approach enables three-dimensional (3D) environmental reconstruction and enhanced target tracking, which are critical for applications such as augmented reality and disaster management.

(4) **Multi-node synchronization and coordination.** Efficient network coordination is pivotal for cooperative sensing. Synchronization protocols, such as time-sensitive networking (TSN), must achieve sub-nanosecond precision across multiple nodes. Cooperative protocols that adaptively allocate roles among transmitting and receiving nodes based on environmental and application demands will be central in ensuring efficient data aggregation and resource utilization. Additionally, cooperative clusters, which group nearby nodes into localized units, can further increase efficiency by enabling intra-cluster coordination and reducing the communication overhead for inter-cluster operations. These clusters facilitate better scalability, allow for localized processing, and increase the robustness of the network by isolating faults to specific clusters without impacting the entire system. 6G cooperative sensing will benefit from multi-hop and mesh network architectures, which allow for the extension of sensing capabilities across larger areas. These architectures will also support the seamless integration of sensing and communication tasks, enabling dynamic reconfiguration of the network in response to changes in topology or user requirements.

(5) **Multi-band sensing for enhanced coverage.** The integration of multi-band sensing capabilities enables systems to utilize diverse frequency bands, optimizing performance under varying conditions. This approach is especially advantageous in environments with high interference or multi-path effects, as it permits the adaptive selection of the most effective frequency bands. Cooperative sensing further increases efficiency by enabling the shared use of sensing and communication spectrums, guided by precise

control technologies. This dual-purpose spectrum utilization not only optimizes resource allocation but also significantly reduces energy consumption when paired with advanced interference-management techniques. Moreover, the integration of passive radar with communication functionalities takes energy efficiency to the next level, enabling deeper spectrum sharing and reducing reliance on active transmissions, thereby offering a sustainable approach to spectrum utilization.

(6) **Multi-modal data fusion for comprehensive insights.** Integrating data from multiple modalities—such as radar, LiDAR, optical sensors, and thermal imaging—significantly increases the robustness and versatility of cooperative sensing systems. Multi-modal fusion not only facilitates comprehensive situational awareness but also overcomes individual sensor limitations, such as radar's inability to capture visual details or cameras' sensitivity to lighting conditions. For instance, in drone sensing scenarios, cooperative sensing leverages standard interfaces to integrate Global Positioning System (GPS), BeiDou, gyroscope, and barometer data, enabling richer contextual insights such as environmental dynamics and object classification. This improved precision bolsters real-time decision-making, supports advanced access management, and allows for ultra-remote control services. Additionally, supplying cross-modal electromagnetic sensing data to large AI models unlocks unprecedented potential for fluid, intuitive human–machine interactions, paving the way for breakthrough applications in autonomous systems and smart environments. Multi-modal integration thus establishes a scalable, high-reliability foundation for tackling dynamic and complex challenges across diverse sectors.

(7) **3D environmental reconstruction.** Cooperative sensing systems can achieve superior spatial and temporal resolution by integrating data from multiple stations and angles. This approach, when augmented with large-scale 3D electromagnetic environmental reconstruction technology, enables the creation of an all-domain, continuous, and fully connected foundation for interactions between the physical and digital worlds. Furthermore, cooperative sensing can empower 3D digital-environment reconstruction to support critical infrastructure for an aging society, providing digital solutions that increase accessibility, safety, and efficiency. This capability not only improves 3D environmental reconstruction and advanced target tracking but also addresses societal challenges, such as elder care, through augmented-reality applications and disaster-management systems.

8. Conclusions

This paper provided an overview of 6G cooperative ISAC, including scenarios and motivations, concepts and models, key technologies, an evaluation framework, a system-level simulation, and a field trial. The historical research trend in this field was introduced, showing how communication and sensing have developed into a cooperative paradigm and how these functions assist each other. Cooperative ISAC is considered to have wider and deeper significance than the traditional multistatic radar system, in that it has four core characteristics, denoted herein as network-enabled, integrated, cooperation, and everything. The key technologies of cooperative ISAC were introduced; we have and will make continuous efforts to advance them. Considering the special architecture and features of cooperative ISAC, we designed a novel performance evaluation framework suitable for it. The system-level evaluation and field trial showed the improved performance of cooperative ISAC. Our future work will focus on the future directions mentioned in this paper, as well as on promoting the standardization and commercialization of cooperative ISAC.

CRediT authorship contribution statement

Guangyi Liu: Supervision, Conceptualization. **Lincong Han:** Writing – original draft, Methodology, Investigation. **Rongyan Xi:** Writing – original draft, Resources. **Liang Ma:** Writing – original draft. **Zixiang Han:** Writing – original draft. **Yahui Xue:** Resources. **Hanting Zhao:** Investigation. **Jing Jin:** Supervision, Conceptualization. **Qixing Wang:** Supervision. **Fei Xu:** Investigation, Funding acquisition.

Declaration of competing interest

The authors declare that they have no known competing financial interests or personal relationships that could have appeared to influence the work reported in this paper.

Acknowledgments

Fei Xu acknowledges funding from China Mobile Communications Group Co., Ltd. We thank Ericsson and the University of Electronic Science and Technology of China for their corporation.

References

[1] Zhang Z, Xiao Y, Ma Z, Xiao M, Ding Z, Lei X, et al. 6G wireless networks: vision, requirements, architecture, and key technologies. IEEE Veh Technol Mag 2019;14(3):28–41.
[2] Liu G, Huang Y, Li N, Dong J, Jin J, Wang Q, et al. Vision, requirements and network architecture of 6G mobile network beyond 2030. China Commun 2020;17(9):92–104.
[3] Fei Z, Wang X, Wu N, Huang J, Zhang JA. Air–ground integrated sensing and communications: opportunities and challenges. IEEE Commun Mag 2023;61(5):55–61.
[4] Yuan W, Liu F, Masouros C, Yuan J, Ng D, Gonzalez PN. Bayesian predictive beamforming for vehicular networks: a low-overhead joint radar-communication approach. IEEE Trans Wirel Commun 2021;20(3):1442–56.
[5] International Telecommunication Union (ITU). Framework and overall objectives of the future development of IMT for 2030 and beyond. New York City: International Telecommunication Union (ITU); 2023.
[6] González-Prelcic N, Furkan Keskin M, Kaltiokallio O, Valkama M, Dardari D, Shen X, et al. The integrated sensing and communication revolution for 6G: vision, techniques, and applications. Proc IEEE 2024;112(7):676–723.
[7] Wang Z, Han K, Jiang J, Wei Z, Zhu G, Feng Z. Symbiotic sensing and communications towards 6G: vision, applications, and technology trends. In: Proceedings of the 94th Vehicular Technology Conference; 2021 Sep 27–30; Norman, OK, USA. New York City: IEEE; 2021. p. 1–5.
[8] Zhang R, Jiang C, Wu S, Zhou Q, Jing X, Mu J. Wi-Fi sensing for joint gesture recognition and human identification from few samples in human–computer interaction. IEEE J Sel Areas Commun 2022;40(7):2193–205.
[9] Kaushik A, Singh R, Li M, Luo H, Dayarathna S, Senanayake R, et al. Integrated sensing and communications for IoT: synergies with key 6G technology enablers. IEEE Internet Things Mag 2024;7(5):136–43.
[10] Lyu Z, Zhu G, Xu J. Joint maneuver and beamforming design for UAV-enabled integrated sensing and communication. IEEE Trans Wirel Commun 2023;22(4):2424–40.
[11] Cheng X, Duan D, Gao S, Yang L. Integrated sensing and communications (ISAC) for vehicular communication networks (VCN). IEEE Internet Things J 2022;9(23):23441–51.
[12] Cao D, Wu M, Gu N, Sherratt R, Ghosh U, Sharma P. Joint optimization of computation offloading and resource allocation considering task prioritization in ISAC-assisted vehicular network. IEEE Internet Things J 2024;11(18):29523–32.
[13] Rou HS, de Abreu GTF, González GD, Gonsa O. Integrated sensing and communications for 3D object imaging via bilinear inference. IEEE Trans Wirel Commun 2024;23(8):8636–53.
[14] Lin B, Zhao C, Gao F, Ye Li G, Qian J, Wang H. Environment reconstruction based on multi-user selection and multi-modal fusion in ISAC. IEEE Trans Wirel Commun 2024;23(10):15083–95.
[15] Skolnik MI. Radar handbook. 3rd ed. New York City: McGraw-Hill; 2008.
[16] Willis NJ, Griffiths HD. Advances in bistatic radar. Raleigh: SciTech Publishing; 2007.
[17] López-Dekker P, Krieger G, Moreira A. Multistatic radar systems. In: D'Errico M, editor. Distributed space missions for Earth system monitoring. New York City: Springer; 2012. p. 61–122.
[18] Stinco P, Greco M, Gini F. Data fusion in a multistatic radar system. In: Proceedings of the International Conference on Synthetic Aperture Sonar and Synthetic Aperture Radar; 2010 Sep 13–14; Lerici, Italy. New York City: IEEE; 2010. p. 13–4.

[19] Park JS, Baek IS, Cho SH. Localizations of multiple targets using multistatic UWB radar systems. In: Proceedings of the 3rd IEEE International Conference on Network Infrastructure and Digital Content; 2012 Sep 21–23; Beijing, China. New York City: IEEE; 2012. p. 586–90.
[20] Ahmed SS, Schmidt LP. Illumination of humans in active millimeter-wave multistatic imaging. In: Proceedings of the 6th European Conference on Antennas and Propagation (EUCAP); 2012 Mar 26–30; Prague, Czech Republic. New York City: IEEE; 2012. p. 1755–57.
[21] Paulraj AJ, Kailath T, inventors; The Board of Trustees of the Leland Stanford Junior University, assignee. Increasing capacity in wireless broadcast systems using distributed transmission/directional reception (DTDR). United States Patent US19920839624. 1994 Sep 6.
[22] Fishler E, Haimovich A, Blum R, Chizhik D, Cimini L, Valenzuela R. MIMO radar: an idea whose time has come. In: Proceedings of the IEEE Radar Conference; 2004 Apr 26–30; Philadelphia, PA, USA. New York City: IEEE; 2004. p. 71–8.
[23] Haimovich AM, Blum RS, Cimini LJ. MIMO radar with widely separated antennas. IEEE Signal Process Mag 2008;25(1):116–29.
[24] Gogineni S, Nehorai A. Target estimation using sparse modeling for distributed MIMO radar. IEEE Trans Signal Process 2011;59(11):5315–25.
[25] Yang C, Han S, Hou X, Molisch AF. How do we design CoMP to achieve its promised potential? IEEE Wirel Commun 2013;20(1):67–74.
[26] Cui Q, Wang H, Hu P, Tao X, Zhang P, Hamalainen J, et al. Evolution of limited-feedback CoMP systems from 4G to 5G: CoMP features and limited-feedback approaches. IEEE Veh Technol Mag 2014;9(3):94–103.
[27] You XH, Wang DM, Sheng B, Gao XQ, Zhao XS, Chen M. Cooperative distributed antenna systems for mobile communications. IEEE Wirel Commun 2010;17(3):35–43.
[28] Ngo HQ, Ashikhmin A, Yang H, Larsson EG, Marzetta TL. Cell-free massive MIMO versus small cells. IEEE Trans Wirel Commun 2017;16(3):1834–50.
[29] Buzzi S, D'Andrea C. Cell-free massive MIMO: user-centric approach. IEEE Wirel Commun Lett 2017;6(6):706–9.
[30] Ngo HQ, Ashikhmin A, Yang H, LarssonEG, Marzetta TL. Cell-free massive MIMO: uniformly great service for everyone. In: Proceedings of the 16th International Workshop on Signal Processing Advances in Wireless Communication (SPAWC); 2015 Jun 28–Jul 1; Stockholm, Sweden. New York City: IEEE; 2015. p. 201–5.
[31] Mealey RM. A method for calculating error probabilities in a radar communication system. IEEE Trans Space Electron Telemetry 1963;9(2):37–42.
[32] Luong NC, Lu X, Hoang DT, Niyato D, Kim DI. Radio resource management in joint radar and communication: a comprehensive survey. IEEE Commun Surv Tutor 2021;23(2):780–814.
[33] Liu F, Masouros C, Petropulu AP, Griffiths H, Hanzo L. Joint radar and communication design: applications, state-of-the-art, and the road ahead. IEEE Trans Commun 2020;68(6):3834–62.
[34] Hassanien A, Amin MG, Zhang YD, Ahmad F. Dual-function radar-communications: information embedding using sidelobe control and waveform diversity. IEEE Trans Signal Process 2015;64(8):2168–81.
[35] Ketonen J, Juntti M, Cavallaro JR. Performance-complexity comparison of receivers for a LTE MIMO-OFDM system. IEEE Trans Signal Process 2010;58(6):3360–72.
[36] Sturm C, Wiesbeck W. Waveform design and signal processing aspects for fusion of wireless communications and radar sensing. Proc IEEE 2011;99(7):1236–59.
[37] BouDaher E, Hassanien A, Aboutanios E, Amin MG. Towards a dual-function MIMO radar-communication system. In: Proceedings of the IEEE Radar Conference; 2016 May 16–20; Philadelphia, PA, USA. New York City: IEEE; 2016. p. 1–6.
[38] Ahmed A, Zhang YD, Himed B. Distributed dual-function radar-communication MIMO system with optimized resource allocation. In: Proceedings of the IEEE Radar Conference; 2019 Apr 23–27; Toulon, France. New York City: IEEE; 2019. p. 15.
[39] Cui Y, Liu F, Jing X, Mu J. Integrating sensing and communications for ubiquitous IoT: applications, trends, and challenges. IEEE Netw 2021;35(5):158–67.
[40] Liu F, Cui Y, Masouros C, Xu J, Han TX, Eldar YC, et al. Integrated sensing and communications: toward dual-functional wireless networks for 6G and beyond. IEEE J Sel Areas Commun 2022;40(6):1728–67.
[41] Wang X, Han L, Xi R, Ma L, Lou M, Jin J. Multipath-exploited bistatic sensing with LoS blockage in MIMO-OFDM systems for 6G. In: Proceedings of the IEEE International Conference on Communication Workshops; 2024 Jun 9–13; Denver, CO, USA. New York City: IEEE; 2024. p. 1529–34.
[42] China Mobile Communications Corporation. Networked cooperative ISAC technologies. Beijing: China Mobile Communications Corporation; 2023. Chinese.
[43] Liu G, Xi R, Han Z, Han L, Zhang X, Ma L. Cooperative sensing for 6G mobile cellular networks: feasibility, performance and field trial. IEEE J Sel Areas Commun 2024;42(10):2863–76.
[44] Jiang T, Zhang J, Tang P, Tian L, Zheng Y, Dou J, et al. 3GPP standardized 5G channel model for IIoT scenarios: a survey. IEEE Internet Things J 2021;8(11):8799–815.
[45] Zhang J, Zhang Y, Yu Y, Xu R, Zheng Q, Zhang P. 3D MIMO: how much does it meet our expectations observed from channel measurements? IEEE J Sel Areas Commun 2017;35(8):1887–903.
[46] Zhang J, Pan C, Pei F, Liu G, Cheng X. Three-dimensional fading channel models: a survey of elevation angle research. IEEE Commun Mag 2014;52(6):218–26.
[47] Liu Y, Zhang J, Zhang Y, Yuan Z, Liu G. A shared cluster-based stochastic channel model for integrated sensing and communication systems. IEEE Trans Veh Technol 2024;73(5):6032–44.
[48] Zhang J, Wang J, Zhang Y, Liu Y, Chai Z, Liu G, et al. Integrated sensing and communication channel: measurements, characteristics and modeling. IEEE Commun Mag 2024;62(6):98–104.
[49] Li R, Xiao Z, Zeng Y. Toward seamless sensing coverage for cellular multi-static integrated sensing and communication. IEEE Trans Wirel Commun 2024;23(6):5363–76.
[50] Gan X, Huang C, Yang Z, Chen X, He J, Zhang Z, et al. Coverage and rate analysis for integrated sensing and communication networks. IEEE J Sel Areas Commun 2024;42(9):2213–27.
[51] Sadeghi M, Behnia F, Amiri R, Farina A. Target localization geometry gain in distributed MIMO radar. IEEE Trans Signal Process 2021;69:1642–52.
[52] Lu B, Wei Z, Wu H, Zeng X, Wang L, Liu X. Deep learning based multi-node ISAC 4D environmental reconstruction with uplink–downlink cooperation. IEEE Internet Things J 2024;11(24):39512–26.
[53] Wang X, Han Z, Jin J, Xi R, Wang Y, Han L, et al. Multistatic integrated sensing and communication system based on macro–micro cooperation. Sensors 2024;24(8):2498.
[54] Wei Z, Liu H, Feng Z, Wu H, Liu F, Zhang Q, et al. Deep cooperation in ISAC system: resource, node and infrastructure perspectives. IEEE Internet Things Mag 2024;7(6):118–25.
[55] Cheng W, Zhao Z, Yang HH, Hong W, Quek TQS, Ding Z. On the study of success serving probability for integrated sensing and communication (ISAC) based on stochastic geometry. In: Proceedings of the IEEE International Conference on Communication; 2024 Jun 9–13; Denver, CO, USA. New York City: IEEE; 2024. p. 5098–103.
[56] Han Z, Ding H, Han L, Ma L, Zhang X, Lou M, et al. Cellular network based multistatic integrated sensing and communication systems. IET Commun 2024;18(20):1878–88.
[57] Wang XY, Yang S, Zhang J, Masouros C, Zhang P. Clutter suppression, time–frequency synchronization, and sensing parameter association in asynchronous perceptive vehicular networks. IEEE J Sel Areas Commun 2024;42(10):2719–36.
[58] Niu Y, Wei Z, Wang L, Wu H, Feng Z. Interference management for integrated sensing and communication systems: a survey. IEEE Internet Things J 2024;12(7):8110–34.
[59] Meng K, Masouros C, Chen G, Liu F. Network-level integrated sensing and communication: interference management and BS coordination using stochastic geometry. IEEE Trans Wirel Commun 2024;23(12 Pt 2):19365–81.
[60] Wang B, Wang Y, Li N, Zhu J, She X, Chen P. On collaborative sensing of cellular networks under mutual signal interference. IEEE Wirel Commun Lett 2024;13(9):2531–5.
[61] Jiang W, Wei Z, Liu F, Feng Z, Zhang P. Collaborative precoding design for adjacent integrated sensing and communication base stations. IEEE Internet Things J 2024;11(9):15059–74.
[62] Liao B, Ngo HQ, Matthaiou M, Smith PJ. Power allocation for massive MIMO-ISAC systems. IEEE Trans Wirel Commun 2024;23(10):14232–48.
[63] Figueroa MR, Bishoyi PK, Petrova M. Power allocation scheme for device-free localization in 6G ISAC networks. In: Proceedings of the IEEE 4th International Symposium on Joint Communication and Sensing; 2024 Mar 19–21; Leuven, Belgium. New York City: IEEE; 2024. p. 1–6.
[64] Liu G, Ma L, Xue Y, Han L, Xi R, Han Z, et al. SensCAP: a systematic sensing capability performance metric for 6G ISAC. IEEE Internet Things J 2024;11(18):29438–54.
[65] Wang X, Han Z, Xi R, Liu G, Han L, Jin J, et al. Cooperative integrated sensing and communication in 6G: from operators perspective. IEEE Wirel Commun 2025;32(1):52–9.
[66] Lotfi P, Soltani S, Murch RD. Printed endfire beam-steerable pixel antenna. IEEE Trans Antennas Propag 2017;65(8):3913–23.
[67] European Telecommunications Standards Institute. TS 38.214: Physical layer procedures for data (Release18). ETSI standard. Paris: 3rd Generation Partnership Project (3GPP); 2024.
[68] Canil M, Pegoraro J, Lacruz JO, Mezzavilla M. An experimental prototype for multistatic asynchronous ISAC. In: Proceedings of the First ACM Workshop on mmWave Sensing System Applications; 2023 Nov 12; Istanbul, Turkiye. New York City: Association for Computing Machinery (ACM); 2023. p. 16–17.
[69] Xie L, Song S, Eldar YC, Letaief KB. Collaborative sensing in perceptive mobile networks opportunities and challenges. IEEE Wirel Commun 2023;30(1):16–23.
[70] Han L, Xue Y, Dong J, Jin J, Wang Q. Networking design and performance evaluation for ISAC in 6G cellular networks. In: Yang Z, Sun G, editors. Proceedings of the 2nd International Conference on Networks, Communications and Intelligent Computing; 2024 Nov 22–25; Beijing, China. Berlin: Springer; 2024.p.157–66.